Biophysical Journal Volume 68 April 1995 1246–1269

An Easy-to-Use Model for O_2 Supply to Red Muscle. Validity of Assumptions, Sensitivity to Errors in Data

K. Groebe*
Institut für Physiologie und Pathophysiologie, Johannes Gutenberg-Universität Mainz, Duesbergweg 6, D-55099 Mainz, Germany

ABSTRACT An easy-to-use capillary cylinder model of O_2 supply to muscle is presented that considers all those factors that are known to be most important for realistic results: (1) red blood cell (RBC) O_2 unloading along the capillary, (2) effects of the particulate nature of blood, (3) free and hemoglobin-facilitated O_2 diffusion and reaction kinetics inside RBCs, (4) free and myoglobin–facilitated O_2 diffusion inside the muscle cell, and (5) carrier-free region separating RBC and tissue. In a first approach, a highly simplified yet reasonably accurate treatment of the complex three-dimensional oxygen diffusion field in and next to capillaries is employed. As an alternative, a more realistic description using RBC/capillary diffusing capacity has been included. Model development proceeds step by step and is designed to be easily comprehensible for a broad readership. In spite of the number of features accounted for, the model is simple to apply, even for scientists not specialized in the field of modeling. P_{O_2} distributions calculated by the model are in good qualitative agreement with experimental data and with former modelling results. By means of suitable extensions to the model that are also developed it is shown for a wide range of muscle performances that quite generally the following complication may be neglected safely: (1) complexity of O_2 diffusion field near capillaries, (2) deviations of capillary domain cross sections from the circular shape, (3) O_2 diffusion parallel to the capillary direction, and (4) P_{O_2} dependence of O_2 consumption rate. Finally, a sensitivity analysis is performed in which propagation of errors in the input data into the results is investigated. The interpretation of the calculated sensitivities gives insights in the specific dependencies of muscular O_2 supply on the various input parameters. Moreover, basic interrelations governing carrier-facilitated diffusional O_2 transport to muscle become apparent and are discussed.

INTRODUCTION

Oxygen supply to red muscle is of great physiological interest, mainly for two reasons: One of the vital organs, the heart, is a red muscle, and lack of oxygen is the primary reason for heart failure. Secondly, skeletal muscle is unique among biological tissues in that its oxygen consumption rate can change 60–80 fold.

O_2 unloading from red blood cells (RBCs) and diffusional O_2 transport in red muscle is a highly complex process that—at high O_2 consumption rates—brings about very characteristic O_2 partial pressure (P_{O_2}) distributions: Next to capillaries there are steep P_{O_2} drops, and P_{O_2} variations in the rest of the muscle are small at low P_{O_2} levels (Gayeski and Honig, 1986, 1988). Using mathematical models, the measured P_{O_2} distributions have been shown to be in accord with predictions from diffusion theory (Federspiel, 1986; Groebe and Thews, 1986, 1990a, 1990b; Groebe, 1990).

In view of the many former theoretical investigations on muscle O_2 supply one might ask: Why develop another model for the same physiological situation? Here are some of the considerations that led to devising the present model:

- The studies cited above have shown that it is important for a realistic description of muscle O_2 supply to consider features such as red cell spacing or carrier-free region (see below) that have not been included in former models.
- The above models also exhibit some problems that render them less suited for routine applications: The model of Federspiel (1986) only implicitly accounts for a carrier-free region; the approach by Groebe and Thews (1986, 1990a, 1990b) has been designed for maximally working muscle exclusively and does not allow for red cell O_2 unloading along capillaries; the model of Groebe (1990) allows for assessing fairly complex physiological situations and uses information on vascular geometries and flows as inputs, quantitative data on which are not routinely available.
- All these models are of high mathematical and computational complexity requiring large amounts of programming effort and computing time.
- There are a number of reasons that make it desirable to have a less complex model available that can also furnish an adequate description of muscle O_2 transport at a physiological range of performances: for example, statistical evaluations of the effects of large-scale heterogeneities (i.e., heterogeneities that are not partly compensated for by O_2 diffusion from better- to worse-supplied capillary domains) that require great numbers of computations; assessment of the impact of one or the other individual factor upon the resulting P_{O_2} profiles for which purpose maximal

Received for publication 1 September 1994 and in final form 17 January 1995

*This work is dedicated to my teacher, Prof. Dr. Dr. G. Thews, on the occasion of his retirement.

Address reprint requests to Address reprint requests to Dr. Karlfried Groebe, Institut für Physiologie und Pathophysiologie, Johannes Gutenberg-Universität Mainz, Duesbergweg 6, D-55099 Mainz, Germany. Tel.: 49 6131 395777; Fax: 49 6131 395774; E-mail: thews@mzdmza.zdv.uni-mainz.de.

0006-3495/95/04/1246/24 $2.00

transparency of the model is needed; computations of P_{O_2} profiles for actual experimental boundary conditions that require a model which is easy to apply. With these kinds of applications in mind, the present model was designed.

The most commonly used model, the classical Krogh model, is not well suited to describe muscle P_{O_2} profiles, as it does not account for the particulate nature of blood, for facilitation of O_2 transport by the oxygen carrier myoglobin (Mb), and for a carrier-free region (CFR) separating red blood cells and muscle fiber (and consisting of a perierythrocytic plasma sleeve, the capillary endothelium, and the interstitial space). It is the objective of the present investigation to present a model of moderate mathematical complexity that is based on and extends the Kroghian approach and that takes into account the following characteristics of muscle O_2 supply:

1. RBC O_2 unloading along the capillary,
2. Effects of the particulate nature of blood, optionally based on a highly realistic approach using RBC/capillary diffusing capacities,
3. Effects of RBC movement with respect to surrounding tissue (optional),
4. Free and hemoglobin-facilitated O_2 diffusion and reaction kinetics inside RBCs,
5. Free and myoglobin-facilitated O_2 diffusion inside the tissue,
6. Free O_2 diffusion in the carrier-free region separating RBC and tissue,
7. Capillary-to-fiber ratio of 1 or, optionally, of 2,
8. Diffusional O_2 transport in parallel with the capillary direction (optional).

Model equations are developed in a way that is intended to be as transparent as possible. Moreover, step-by-step instructions on how to program the model on a computer are included in an appendix.

Following model formulation, the importance of considering microvascular geometries in muscles with capillary-to-fiber (c/f) ratios other than 1 (which is the straightforward case), diffusion in parallel with the capillary direction, and P_{O_2} dependence of local O_2 consumption rate are assessed. Wherever appropriate, this is done by means of histograms of the tissue P_{O_2} probability distribution.

For an adequate interpretation of modeling results, it is essential to consider how sensitive calculated P_{O_2} distributions are to known uncertainties in the input data propagated into the outcomes. Vice versa, when one is experimentally determining parameter values that are going to be used as input data in O_2 supply models it is important to know to what precision the individual parameters are required to be correct in order to keep errors in the results below a given limit. Motivated by this kind of question, in a final section I present a first-order sensitivity analysis for parameter dependence of P_{O_2} profiles in which the derivatives of tissue P_{O_2} with respect to the various parameters are calculated. This type of analysis allows for an interpretation of the numerical results in terms of general principles governing muscle O_2 supply in given physiological situations.

ANALYSIS AND DATA

1. Formulation of the mathematical problem

In the following, it is assumed that the tissue to be modeled is in steady state throughout and that it holds parallel capillaries of outer radius R_{CFR} (μm) and of length L (μm), each of which supplies a well-defined capillary domain with oxygen (see schematic drawing in Fig. 1). Let the functional capillary density fcd be defined as number of capillaries open to red cells per square millimeter of cross-sectional area in sections positioned perpendicular to the capillary direction. Consequently, the average cross sectional area of each capillary domain is $A = 10^6/\text{fcd}$ (μm^2). (At low values of capillary P_{O_2} not all of a capillary domain may be well oxygenated. Therefore, actual A may need to be set to accordingly smaller values if capillary P_{O_2} becomes too low to supply the entire domain.) Assume that the muscle is perfused with blood of hematocrit Hct at a rate of $\dot{Q}$ (ml)100 g)$^{-1}$ min^{-1}), corresponding to an average capillary blood flow rate $\dot{Q}_{Cap} = 1.77 \times 10^{-4}\ \dot{Q}AL$ (fl/s). In this equation, minutes have been converted to seconds and a specific tissue gravity of 1.06 kg/l (Mendez and Keys, 1960) has been used.

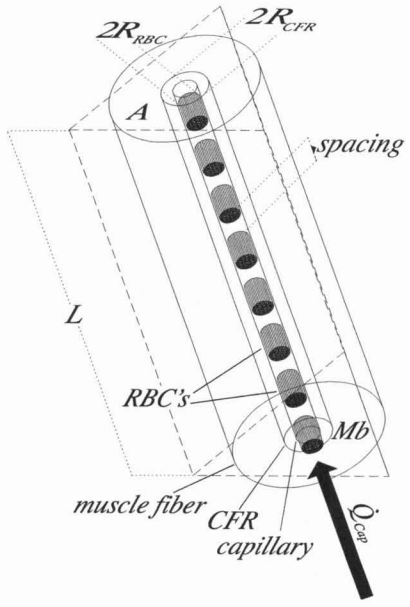

FIGURE 1 Schematic drawing of capillary domain geometry in muscle. A capillary domain (large circular or triangular cylinder) of length L and cross-sectional area A is supplied out of a central capillary, which is perfused by a given blood flow $\dot{Q}_{Cap}$. Adjacent red blood cells (RBCs, radius R_{RBC}) within the capillary are separated by plasma-filled gaps ("spacing"). Most of the capillary domain is occupied by the muscle fibers in which myoglobin (Mb) serves as an oxygen carrier. Erythrocytes and muscle fiber are separated by a carrier-free region (CFR, radius R_{CFR}), which is made up of a perierythrocytic plasma sleeve, the capillary endothelium, and interstitial space.

As muscle capillaries are very narrow, RBCs travel predominantly in single-file flow with plasma-filled gaps ("spacing") between adjacent red cells. It was Hellums (1977) who pointed out that this observation should have important consequences for O_2 unloading because only part of the capillary surface is maximally effective in O_2 exchange. In the following, the fraction of the capillary length occupied by erythrocytes is denoted by l_{RBC}.

Within the muscle cells, myoglobin (Mb) at a concentration of C_{Mb} (mol/l) is present, which serves as an oxygen carrier. Similarly, oxygen transport is facilitated by hemoglobin (Hb) contained in the erythrocytes at a concentration of C_{Hb} (mol/l). RBCs are assumed cylindrical of radius R_{RBC} (μm), which is related to red cell volume V_{RBC} (fl) and length L_{RBC} (μm) as $R_{RBC} = \sqrt{V_{RBC}\pi^{-1}L_{RBC}^{-1}}$. In a layer surrounding the erythrocytes ($R_{RBC} < r \leq R_{CFR}$), the thickness of which is $d_{CFR} = R_{CFR} - R_{RBC}$ (μm) and which consists of a peri-erythrocytic plasma sleeve, the capillary endothelium, and the interstitial space, no oxygen carrier is present (carrier-free region, CFR), and oxygen is therefore transported by free O_2 diffusion only.

Let the overall O_2 consumption rate in the muscle be $\dot{V}_{O_2}$ (ml O_2 (100 g)$^{-1}$ min^{-1}). As oxygen is consumed predominantly within the muscle cells, we have to correct this figure for the extracellular volume (and to convert units similarly as for $\dot{Q}$ above), yielding an effective parenchymal O_2 consumption rate

$$\dot{V}_{O_2} = 7.89 \times 10^{-6}\left(1 - \frac{\pi R_{CFR}^2}{A}\right)^{-1} \dot{V}_{O_2}\left(\frac{\text{mol}}{\text{ls}}\right).$$

According to Fick's first law of diffusion, diffusional O_2 flux density (the O_2 flux per unit area normal to the direction of the flux) is equal to the P_{O_2} gradient times the O_2 conductivity K_{O_2}, which is the product of O_2 diffusion coefficient D and O_2 solubility α in the medium. Therefore, in order to formulate the mathematical problem, we need to introduce the following additional notation: O_2 diffusion coefficients D_M, D_{CFR}, and D_{RBC} (μm^2/s) and (physical) O_2 solubilities α_M, α_{CFR}, α_{RBC}, and α_{Blood} (mol l^{-1}mm Hg^{-1}). Subscripts M, CFR, RBC, and Blood refer to muscle fiber, carrier-free region, erythrocyte, and whole blood, respectively. D_{Mb} is the diffusion coefficient (μm^2/s) of Mb in the fiber. Frequently, diffusion coefficients and solubilities are given in units other than the above. These may be converted according to D (μm^2/s) = $10^8 \times D$ (cm^2/s) and α (mol l^{-1}mm Hg^{-1}) = 0.0446α (ml O_2 ml^{-1}mm Hg^{-1}) = $5.87 \times 10^{-5}\alpha$ (ml O_2 ml^{-1}atm^{-1}).

A cylindrical coordinate system (r, φ, z) is introduced that is arranged such that its origin is located in the center of the beginning of a straight capillary and that its z axis is aligned with the capillary direction. The z direction will also be referred to as "longitudinal" or "axial" and any direction perpendicular to it as "transversal."

Blood O_2 content at O_2 partial pressure P is denoted by $\mathscr{C} = \mathscr{C}(P)$ (mol l^{-1}). $\mathscr{C}$ is made up of O_2 bound to Hb and of O_2 in physical solution:

$$\mathscr{C}(P) = Hct\, C_{Hb}\mathscr{S}(P) + \alpha_{Blood}P, \qquad (1)$$

where $\mathscr{S}(P)$ is the Hb-O_2 saturation at P. Hemoglobin O_2 saturation $\mathscr{S}$ and its equilibrium P_{O_2} are related via the Hb-O_2 dissociation curve, the Hill approximation to which we are going to use:

$$\mathscr{S}(P) = \frac{(P/\mathscr{P}_{50})^n}{1 + (P/\mathscr{P}_{50})^n}$$

with the inverse (2)

$$\mathscr{P}(\mathscr{S}) = \mathscr{P}_{50}\sqrt[n]{\frac{\mathscr{S}}{1-\mathscr{S}}},$$

where $\mathscr{P}_{50}$ is the half-saturation P_{O_2} of Hb and n is the Hill coefficient. As even during O_2 unloading the bulk of blood Hb is in equilibrium with O_2 (cf. Groebe and Thews, 1986), Eq. 2 may be applied for relating mean capillary blood O_2 saturation (or content) to mean capillary blood P_{O_2}. Substituting $\mathscr{S}$ into Eq. 1 according to Eq. 2, we may express blood O_2 content as

$$\mathscr{C}(P) = Hct\, C_{Hb}\frac{(P/\mathscr{P}_{50})^n}{1 + (P/\mathscr{P}_{50})^n} + \alpha_{Blood}P. \qquad (3)$$

Even though physically dissolved oxygen may usually be neglected compared with Hb-bound O_2, the term $\alpha_{Blood}P$ has been retained in Eq. 3. This allows one to apply the model to Hb-free perfused muscle by setting C_{Hb} to zero.

In the following, the equilibrium P_{O_2} pertinent to a blood O_2 content $\mathscr{C}$—which is denoted by $\tilde{\mathscr{P}} = \mathscr{P}(\mathscr{C})$—will be needed. Because of the difference in their arguments there is no risk of confusing $\mathscr{P}(\mathscr{C})$ with the inverse of the Hb–O_2 dissociation curve, $\mathscr{P}(\mathscr{S})$. Therefore, the same symbol has been employed. $\mathscr{P}(\mathscr{C})$ is obtained by inversion of Eq. 3. Note that there exists no analytical expression for $\mathscr{P}(\mathscr{C})$ in the general case. If physically dissolved O_2 is to be neglected or if $C_{Hb} = 0$, $\mathscr{P}(\mathscr{C})$ is given by

$$\mathscr{P}(\mathscr{C}) = \mathscr{P}_{50}\sqrt[n]{\frac{\mathscr{C}}{Hct\, C_{Hb} - \mathscr{C}}} \quad \text{or} \quad \mathscr{P}(\mathscr{C}) = \frac{\mathscr{C}}{\alpha_{Blood}}, \qquad (4)$$

respectively. In the general case under normal conditions, $\mathscr{P}(\mathscr{C})$ is close to the result from the first of Eqs. 4, which may serve as initial approximation in a numerical algorithm suitable for solving Eq. 3.

From experimental (Gayeski and Honig, 1988) as well as theoretical (Groebe, 1990, and the Results and Specific Discussion section, subsection 3) studies it is known that in muscle P_{O_2} gradients along the capillary direction are trivial compared with radial gradients, and therefore axial diffusion is neglected. This assumption is made for the CFR and the capillary as well. With these definitions and simplifying assumptions, steady-state O_2 diffusion in muscle fiber and CFR is described by the well-known partial differential equations

$$D_M\alpha_M\nabla^2 P + D_{Mb}C_{Mb}\nabla^2 S = \dot{V}_{O_2} \quad \text{in the muscle cells} \qquad (5)$$

$$\nabla^2 P = 0 \quad \text{in the carrier-free region,} \qquad (6)$$

where P is the O_2 partial pressure, S is the myoglobin O_2 saturation, and ∇^2 is the two-dimensional Laplace operator in cross sections perpendicular to the capillary direction. The reaction between Mb and O_2 is assumed to reside in chemical equilibrium, so S is related to P via the Mb oxygen dissociation curve:

$$S(P) = \frac{P}{P + P_{50}}, \tag{7}$$

where P_{50} is the half-saturation P_{O_2} of Mb. Note that, other than described by Fick's laws of diffusion in carrier-free tissue, P_{O_2} gradients in muscle cells depend not only on $\dot{V}_{O_2}$ and tissue O_2 conductivity $D_M\alpha_M$ but—via the Mb oxygen dissociation curve—also on actual P_{O_2} and on diffusivity and concentration of Mb (cf. Eq. 5). For this situation, K_{O_2}—the factor of proportionality between P_{O_2} gradient and O_2 flux density—is a function of actual P_{O_2} that will be denoted "effective O_2 conductivity" (cf. Groebe, 1992). K_{O_2} is given by

$$\begin{aligned} K_{O_2}(P) &= D_M\alpha_M\left(1 + \frac{D_{Mb}C_{Mb}}{D_M\alpha_M}S'(P)\right) \\ &= D_M\alpha_M\left(1 + \frac{D_{Mb}C_{Mb}}{D_M\alpha_M}\frac{P_{50}}{(P + P_{50})^2}\right) \end{aligned} \tag{8}$$

and is graphed in Fig. 2 (solid curve). Effective O_2 conductivity is equal to free O_2 conductivity $D_M\alpha_M$ (dotted line in Fig. 2) at very high values of P_{O_2} and increases with falling P_{O_2} to approximately six times $D_M\alpha_M$ at $P = 0$ mm Hg.

Within capillary and CFR, the oxygen diffusion field is of considerable complexity. In the real situation, oxygen leaves the red cell mainly in radial direction, to a small portion also in longitudinal direction across the front and back ends of the RBC, and from there through the intererythrocytic plasma gap (Fig. 3 *a*). Moreover, red cells move relative to the capillary and the surrounding tissue and "charge" their vicinity with oxygen, which is released when a plasma gap passes by. In former models of tissue O_2 supply, red cell spacing was mostly neglected and a homogeneous O_2 flux out of the capillary was assumed, just as if the capillary were perfused with hemoglobin solution (Fig. 3 *b*). An upper bound on the effects of red cell spacing may be found by assuming that O_2 flux is exclusively radial but present only adjacent to capillary locations at which erythrocytes reside (Fig. 3 *c*)—which greatly overestimates radial O_2 flux densities and P_{O_2} drops. Because for the purpose of the present study the above simplifying assumptions were too inaccurate on the one hand, and treatment of the full two-dimensional boundary value problem in the transition region between red cells and muscle fiber did not appear to be feasible on the other, a simple yet reasonably precise approximate procedure for dealing with RBC spacing was sought. One possible approach (which is used in the following) has been suggested by Hellums (1977) and has been evaluated by Groebe and Thews (1990a), who showed that assuming radial O_2 flux in the CFR adjacent to RBCs only, and uniform radial O_2 flux in the muscle fiber (Fig. 3 *d*) gives results that are very similar to the ones from a three-dimensional solution of the diffusion equation. With these assumptions one overestimates O_2 flux densities and P_{O_2} gradients in the CFR and underestimates them in fiber regions located next to the capillary, the effects of which roughly cancel. Another approach is detailed in subsection 6 and uses diffusing capacities that are obtained from a solution of the full two-dimensional time-dependent differential equation of red cell O_2 unloading under capillary conditions.

For the solution of the above diffusion problem we require the following boundary and interface conditions

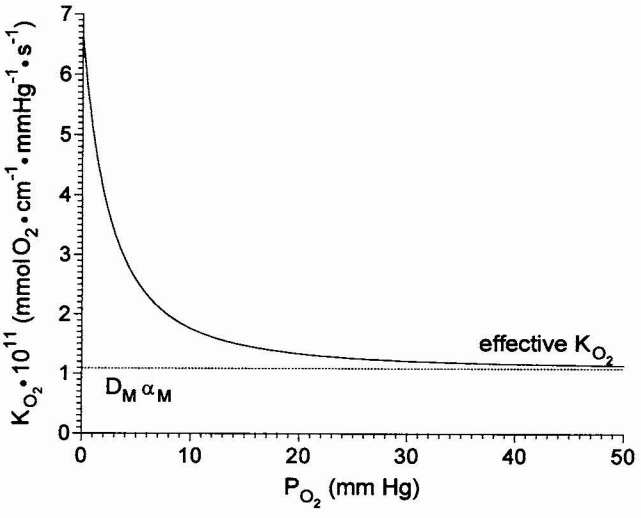

FIGURE 2 P_{O_2} dependence of effective O_2 conductivity in the presence of myoglobin (effective K_{O_2}). At high P_{O_2}, effective conductivity is almost equal to the one for free O_2 diffusion (dotted horizontal line), and it becomes maximal at very small values of P_{O_2}.

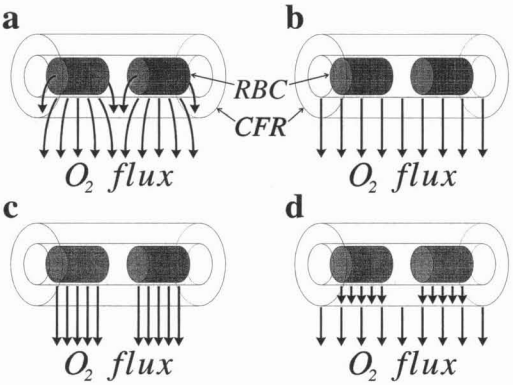

FIGURE 3 Different treatments of O_2 fluxes (bold arrows) in and next to capillaries. (*a*) In the real situation, oxygen leaves the red cell mainly in radial direction, to a small portion also in longitudinal direction through the front and back ends of the RBC, and through the intererythrocytic plasma gap. (*b*) Red cell spacing is neglected and a homogeneous O_2 flux out of the capillary is assumed, just as if the capillary were perfused with hemoglobin solution (Krogh's approach). (*c*) A (very rough) upper bound on the effects of red cell spacing is found by assuming that O_2 flux is exclusively radial but present only adjacent to capillary locations at which erythrocytes reside. (*d*) The present model assumes radial O_2 flux in the CFR adjacent to RBC's only, and uniform radial O_2 flux in the muscle fiber.

to be satisfied:

1. The O_2 flux across the outer boundary of the capillary domain is to vanish.
2. At the interface between CFR and flowing RBCs (i.e., at the RBC membrane), P has to be continuous and transcapillary O_2 flux Φ_C (i.e., the oxygen unloaded from the blood per unit length (u.l.) of capillary and unit of time) needs to be matched to the O_2 consumed per u.l. of capillary domain and unit of time:

$$\underbrace{\dot{V}_{O_2}(A - \pi R_{CFR}^2)}_{\substack{O_2 \text{ consumed per u.l.} \\ \text{of capillary domain} \\ \text{and unit of time}}} = \Phi_C = \underbrace{-\dot{Q}_{Cap}\frac{d\mathscr{C}}{dz}}_{\substack{O_2 \text{ unloaded per} \\ \text{u.l. of capillary} \\ \text{and unit of time}}}, \quad (9)$$

   where $d\mathscr{C}/dz$ is the change in blood O_2 content along the capillary.
3. Across the interface between CFR and muscle cells (i.e., across the sarcolemma), P as well as the O_2 flux densities in the radial direction is to be continuous. In order to keep the mathematical problem easily tractable but nevertheless to take account of the fact that only the fraction l_{RBC} of the capillary length is occupied by RBCs (and therefore is maximally effective in gas exchange; see above), we assume that within the CFR O_2 diffusion is exclusively radial and takes place adjacent to erythrocytes only. For the tissue, we assume that the O_2 flux across the interface is uniform with no differences between locations next to RBCs containing capillary sites and next to plasma gaps. Thus, radial O_2 fluxes per u.l. of capillary on both sides of the capillary–fiber interface become

$$\underbrace{-2\pi R_{CFR}\left(D_M\alpha_M\frac{\partial P}{\partial r}\bigg|_{r=R_{CFR}^+} + D_{Mb}C_{Mb}\frac{\partial S}{\partial r}\bigg|_{r=R_{CFR}^+}\right)}_{\text{in the fiber}} = \dot{V}_{O_2}(A - \pi R_{CFR}^2) = \underbrace{-2\pi R_{CFR} l_{RBC} D_{CFR}\alpha_{CFR}\frac{\partial P}{\partial r}\bigg|_{r=R_{CFR}^-}}_{\text{in the CFR}}. \quad (10)$$

2. Transformation of the diffusion equations 5 and 6

Similarly, as in the models of Hoofd et al. (1989) and Groebe (1990), the "effective partial pressure" P^* and the transformation $\mathbf{P}^*(P)$ are introduced:

$$P^* = \mathbf{P}^*(P) = P + \frac{D_{Mb}C_{Mb}}{D_M\alpha_M}S(P) = P + \frac{D_{Mb}C_{Mb}}{D_M\alpha_M}\frac{P}{P + P_{50}} \quad (11)$$

Substitution in Eq. 5 yields the differential equation

$$\nabla^2 P^* = \frac{\dot{V}_{O_2}}{D_M\alpha_M}. \quad (12)$$

In this equation and in Eq. 6, ∇^2 needs to be expressed in plane polar coordinates, giving

$$\frac{1}{r}\frac{\partial}{\partial r}\left(r\frac{\partial P^*}{\partial r}\right) + \frac{1}{r^2}\frac{\partial^2 P^*}{\partial \varphi^2} = \frac{\dot{V}_{O_2}}{D_M\alpha_M} \quad \text{in the muscle cells} \quad (13)$$

$$\frac{\partial}{\partial r}\left(r\frac{\partial P}{\partial r}\right) + \frac{1}{r}\frac{\partial^2 P}{\partial \varphi^2} = 0 \quad \text{in the CFR.} \quad (14)$$

3. RBC surface P_{O_2}, P_{RBC}

To solve these differential equations in a plane located at longitudinal position z, the P_{O_2} at the RBC surface, P_{RBC}, is required (see the above boundary condition 2.). To obtain P_{RBC} we first need to know the mean capillary blood O_2 content $\mathscr{C}$ at z. Transforming Eq. 9 yields

$$\frac{d\mathscr{C}}{dz} = -\frac{\dot{V}_{O_2}}{\dot{Q}_{Cap}}(A - \pi R_{CFR}^2);$$

thus

$$\mathscr{C}(z) = \mathscr{C}_A - \int_0^z \frac{\dot{V}_{O_2}}{\dot{Q}_{Cap}}(A(\tilde{z}) - \pi R_{CFR}^2)\,d\tilde{z} \left[= \mathscr{C}_A - \frac{\dot{V}_{O_2}}{\dot{Q}_{Cap}}(A - \pi R_{CFR}^2)z\right], \quad (15)$$

where $\mathscr{C}_A$ is the blood O_2 content at the capillary origin. The explicit integration (second equality in brackets) is feasible only if the entire capillary domain is well oxygenated, and hence its cross-sectional area A does not change with longitudinal position. Most commonly, the arterial O_2 saturation $\mathscr{S}_A$ is known rather than $\mathscr{C}_A$. In this case, one obtains the corresponding P_{O_2}, $\mathscr{P}(\mathscr{S}_A)$, from the second of Eqs. 2 and calculates $\mathscr{C}_A$ according to Eq. 3.

Next, the O_2 flux, Φ_{RBC}, out of a RBC has to be determined. Let L_{RBC} be the average distance along the capillary that is occupied by *one single* RBC. As only a fraction l_{RBC} of the total capillary length holds erythrocytes, each RBC—on average—supplies O_2 to a slab of capillary domain the thickness of which is L_{RBC}/l_{RBC}. Using the left-hand side of Eq. 9, we find

$$\Phi_{RBC} = \frac{\dot{V}_{O_2}L_{RBC}}{l_{RBC}}(A - \pi R_{CFR}^2). \quad (16)$$

Clark et al. (1985) have developed an analytical model of RBC O_2 unloading that considers free and hemoglobin-facilitated O_2 diffusion and reaction kinetics inside RBCs and that allows one to calculate the red cell surface P_{O_2} from mean Hb-O_2 saturation $\mathscr{S}$ and red cell O_2 flux Φ_{RBC} (see Clark and Clark 1986):

$$P_{RBC} = \mathscr{P}(\mathscr{C})\left(1 - \frac{\Phi_{RBC}}{\sigma_{RBC}\sqrt{C_{Hb}D_{RBC}\alpha_{RBC}k\mathscr{P}(\mathscr{C})n\mathscr{S}(\mathscr{P}(\mathscr{C}))}}\right), \quad (17)$$

where σ_{RBC} is the red cell surface area, k is the rate constant of

the O_2 dissociation from Hb-O_2, $\mathcal{P}(\mathcal{C})$ is the P_{O_2} pertinent to blood O_2 content $\mathcal{C}$ (as defined in and preceding Eq. 4), and $\mathcal{S}(\mathcal{P}(\mathcal{C}))$ is obtained from $\mathcal{P}(\mathcal{C})$ according to the first of Eqs. 2.

4. Solution of the diffusion equations 13 and 14 for axisymmetric capillary domains

This case represents the classical Krogh geometry in which all derivatives with respect to φ vanish and in which cross sections of capillary domains are circular and of Krogh radius $R_K = \sqrt{A/\pi} = 10^3(\pi \times \text{fcd})^{-1/2}$. By straightforward integration of Eq. 14 one obtains

$$P(r) = c_1 \ln \frac{r}{R_{RBC}} + P_{RBC}. \tag{18}$$

Substituting the derivative of Eq. 18, $P'(R_{CFR}) = c_1/R_{CFR}$, for $\partial P/\partial r|_{r=R_{CFR}^-}$ into the condition for the interface between CFR and fiber (Eq. 10, second equality), one finds c_1, and the resulting P_{O_2} in the CFR is

$$P(r) = P_{RBC} - \frac{\dot{V}_{O_2}(R_K^2 - R_{CFR}^2)}{2D_{CFR}\,\alpha_{CFR}\,l_{RBC}} \ln \frac{r}{R_{RBC}}. \tag{19}$$

Similarly, one obtains by integration of Eq. 13

$$P^*(r) = c_2 \ln \frac{r}{R_{CFR}} + \frac{\dot{V}_{O_2}}{4D_M\,\alpha_M}(r^2 - R_{CFR}^2) + P^*_{CFR},$$

where P^*_{CFR} is the effective partial pressure (defined according to Eq. 11) pertinent to $P(R_{CFR})$ from Eq. 19. By determining c_2 such that the gradient at the outer perimeter of the Krogh cylinder,

$$\left.\frac{dP^*}{dr}\right|_{r=R_K} = \frac{c_2}{R_K} + \frac{\dot{V}_{O_2} R_K}{2D_M\,\alpha_M},$$

vanishes, both the zero flux condition at the outer boundary and (the first equality of) the interface condition Eq. 10 are satisfied, and we have for the effective P_{O_2} inside the muscle cells

$$P^*(r) = P^*_{CFR} + \frac{\dot{V}_{O_2}}{2D_M\,\alpha_M}\left(\frac{1}{2}(r^2 - R_{CFR}^2) - R_K^2 \ln \frac{r}{R_{CFR}}\right). \tag{20}$$

$P^*(r)$ resulting from Eq. 20 is transformed into $P(r)$ by applying the inversion $\mathbf{P}(P^*)$ of $\mathbf{P}^*(P)$ (Eq. 11):

$$P = \mathbf{P}(P^*) = \frac{1}{2}\left(P^* - \frac{D_{Mb}\,C_{Mb}}{D_M\,\alpha_M} - P_{50}\right) + \frac{1}{2}\sqrt{\left(P^* - \frac{D_{Mb}\,C_{Mb}}{D_M\,\alpha_M} - P_{50}\right)^2 + 4P^*P_{50}}. \tag{21}$$

5. Anoxic loci

Only those parts of a capillary domain can be supplied with oxygen in which a sufficiently high P_{O_2} is maintained. This should be considered in the algorithm for calculating P_{O_2} distributions.

Mitochondrial O_2 uptake is virtually unaffected by variations in P_{O_2} unless O_2 partial pressure drops below a critical mitochondrial P_{O_2} (which will be denoted P_{crit}). An upper bound on P_{crit} at maximal O_2 flux is 0.5 mmHg (Gayeski et al., 1987). P_{crit} should be substantially smaller at normal work rates (Connett et al., 1990). As P_{crit} is very small, P_{O_2} values below P_{crit} do not allow for the sizable P_{O_2} gradients that would be necessary to supply significant amounts of more distant fiber portions with oxygen. Therefore, it is adequate to "switch off" O_2 uptake in regions in which P_{O_2} is very low. This simplified treatment of sites of low P_{O_2} is also supported by the experimental observation that during heavy exercise less than 5% of muscle fiber cross sections exhibit P_{O_2} values below 0.5 mmHg in their centers (Gayeski et al., 1987).

To take account of the fact that cell respiration does not stop completely as soon as P_{O_2} falls to P_{crit}, in the model O_2 uptake is turned off at values of P_{O_2} smaller than $P_{crit}/2$. In other words, O_2 consumption rate is assumed constant if $P_{O_2} \geq P_{crit}/2$ and is set to 0 in regions in which P^* falls below $\mathbf{P}^*(P_{crit}/2)$ (the effective P_{O_2} corresponding to $P_{crit}/2$ according to Eq. 11). If at some radial position $P^* < \mathbf{P}^*(P_{crit}2)$, R_K needs to be reduced. Accordingly, the amount of oxygen consumed in the cross section considered is diminished, and hence P_{O_2} drops and $P^*(R_K)$ at the new R_K are changed. As a consequence, in order to determine R_K, the nonlinear equation $P^*(R_K) = P^*(P_{crit}/2)$ (in which $P^*(r)$ is defined by Eqs. 19 and 20) has to be solved. This cannot be done analytically but only numerically. In the case that R_K is not constant all along the capillary but decreases toward the venous capillary end, capillary domain cross-sectional area $A = \pi R_K^2$ also varies along the capillary, and the straightforward longitudinal integration for determining blood O_2 content at z (Eq. 15, second equality) is not feasible. Rather, the integral has to be evaluated numerically using the actual $R_K(z)$. (This affects calculation of the fiber O_2 consumption rate $\dot{V}_{O_2}$ from the given overall O_2 consumption rate $\dot{V}_{O_2}$ and has to be considered if nonnegligible amounts of the tissue fall anoxic. For the data of the present study, P_{O_2} drops below $P_{crit}/2$ only at the highest performance and only in a few percent of the tissue, cf. Fig. 6 below.)

This concludes the description of the basic model. Step-by-step instructions on how to program model equations on a computer are included in Appendix A.

6. Extension: employing red cell diffusing capacity

When formulating the mathematical problem it was mentioned that within the framework of a tissue O_2 supply model, the O_2 transport equation in the transition region between erythrocytes and muscle fiber cannot easily be solved with desirable accuracy. Based on former studies by Hellums (1977) and Groebe and Thews (1990a), a simplified description was employed instead, in which O_2 flux was restricted to locations adjacent to RBC's in the CFR, and was assumed

uniform (with respect to the longitudinal coordinate) in the rest of the tissue.

With this procedure, nonnegligible errors might ensue if intererythrocytic plasma gaps become extraordinarily large as, e.g., in severe anemia. Moreover, periodic storage and release of oxygen in the vicinity of moving erythrocytes are not accounted for. These disadvantages can be avoided if red cell O_2 release is not explicitly calculated as part of the tissue O_2 supply model but rather computed from the results of a model of O_2 unloading under capillary conditions, in which the circumstances within and around the capillary can be reproduced much more accurately. To that end, the results of such a model need to be converted, e.g., into the form of a diffusing capacity of a short capillary segment containing exactly one moving erythrocyte. This has been done by Groebe and Thews (1989) who published diffusing capacities of capillaries containing red cells (which were resting or moving at 4 mm/s) as functions of RBC spacing. Ideally the link between capillary model and tissue model should be located far enough apart from erythrocytes that at the interface temporal and spatial oscillations of P_{O_2} and O_2 flux have largely dissipated.

To incorporate diffusing capacities into the model, some changes have to be made (cf. Federspiel and Popel, 1986): For a capillary blood O_2 content $\mathscr{C}$, P_{O_2} at the interface between CFR and fiber, P_{CFR}, is calculated not from Eq. 19 but according to

$$P_{CFR} = \mathscr{P}(\mathscr{C}) - \frac{\Phi_{RBC}}{\kappa}, \qquad (22)$$

where $\mathscr{P}(\mathscr{C})$ is the P_{O_2} pertinent to $\mathscr{C}$, Φ_{RBC} is the O_2 flux out of the erythrocyte, and κ is the RBC/capillary diffusing capacity. The pertinent effective P_{O_2}, $\mathbf{P}^*(P_{CFR})$, has to be substituted for P^*_{CFR} in Eq. 20. For simplicity of formulation, the link between capillary and tissue models in Eq. 22 has been aligned with the interface between CFR and fiber. Different choices are possible as well, for which, however, an accordingly computed κ has to be employed.

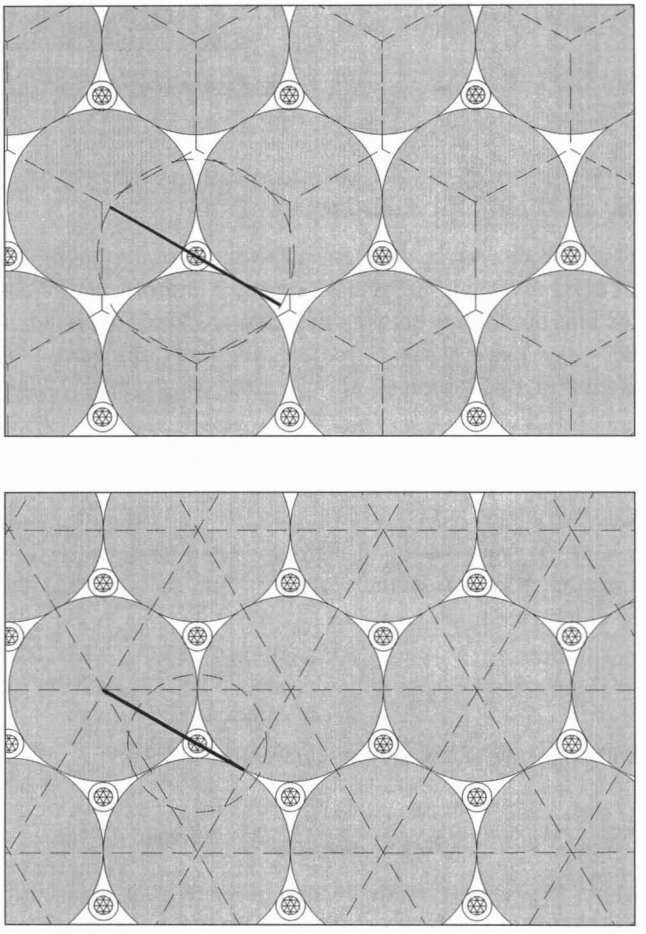

FIGURE 4 Cross sections through idealized muscles exhibiting c/f ratios of 1 (top panel) and of 2 (bottom panel). Large shaded circles, muscle fibers; small circles, capillaries containing RBCs (cross-hatched); dashed hexagons and triangles, capillary domains; dashed circles, Krogh cylinders of same size as capillary domains. P_{O_2} profiles in Fig. 5 have been calculated in longitudinal sections identified by the bold lines.

7. Extension: the solution for a capillary-to-fiber ratio of 2

Before we go into mathematical treatment of this case we first ought to clarify the significance of the capillary-to-fiber (c/f) ratio for O_2 supply. Whereas capillary density determines the average *magnitude* of capillary domains (more precisely, of their cross-sectional areas and hence of transcapillary O_2 flux), the c/f ratio holds information about their *shape*. This is demonstrated in Fig. 4, which displays cross sections through an idealized muscle. The large shaded circles represent the muscle fibers, and the small solid circles are capillaries containing RBCs (cross-hatched), which are surrounded by CFRs. Dashed straight lines delineate capillary domain boundaries. In Fig. 4, top panel, the c/f ratio is 1, and capillary domains have hexagonal shapes. Obviously, these hexagons are well approximated by circles, suggesting that the cylinder geometry should furnish an appropriate description of the physiological situation. In Fig. 4, bottom panel, muscle fibers are unchanged; the capillary density, however, is doubled (and transcapillary O_2 flux is halved). Thus, the c/f ratio is 2 and capillary domains are of triangular shape. Apparently, a cylinder of matching size (dashed circle) represents but a poor approximation to the capillary domain. As typical c/f ratios range between 1 and 2 (see, e.g., Martin et al., 1932) this discrepancy needs further evaluation.

From Eqs. 12 and 13 we see that for any harmonic function $h(r,\varphi)$ (i.e., h satisfying $\nabla^2 h = 0$) $P^* + h$ is still a solution of the diffusion equation. However, $P^* + h$ in general does not satisfy the zero-flux condition at the outer boundary of the capillary domain any more. Vice versa, it is possible to choose harmonic functions $h(r,\varphi)$ such that a zero-flux condition is satisfied on the boundaries of capillary domains of different (e.g., triangular) shapes. Details of the analysis are of technical nature and are given in Appendix B.

8. Extension: the solution for axial diffusion

Capillary P_{O_2} drops as the blood travels down the capillary giving off oxygen. Accordingly, the P_{O_2} in the supplied tissue region also drops, resulting in P_{O_2} gradients in the axial direction of capillary domains that are—in the model considering exclusively radial diffusion—of such magnitude that they should be detectable experimentally. However, these axial P_{O_2} gradients induce O_2 fluxes from the arterial end of the capillary domain toward its venous end. As a consequence, Eq. 9—which requires mass balance of transcapillary O_2 flux Φ_C and O_2 consumption in capillary domain cross sections—is not valid any more. Rather, Φ_C and pericapillary P_{O_2} drops decrease from the arterial to the venous capillary ending, in this way counteracting axial P_{O_2} gradients within the capillary domain. As experimental studies (Gayeski and Honig, 1988) have demonstrated the absence of significant axial gradients that were related to the capillaries, it is of interest to know how effectively axial diffusion can flatten the longitudinal gradient. Furthermore, the consequences of neglecting axial diffusion within capillary domains upon calculated P_{O_2} histograms are to be assessed.

Similarly, as in the previous subsection, the P_{O_2} distribution (more precisely the one of the effective P_{O_2}, P^*) may be composed of a term accounting for O_2 consumption in the tissue plus a sum of appropriately chosen harmonic functions that depend on the radial and longitudinal coordinates. In the present case, however, we may use harmonic functions that satisfy a zero flux condition at the outer boundaries of the capillary domain, so the zero flux boundary condition is automatically met for the composed solution also. The conditions that remain to be satisfied are the continuity of P_{O_2} and O_2 flux across the interface between carrier-free region and muscle cell. This is achieved by an appropriate choice of the coefficients to the harmonic functions and of the local drop in capillary O_2 content along the capillary. Further details of the solution may be found in Appendix B.

9. Extension: P_{O_2} dependence of O_2 consumption rate

As mentioned in subsection 5, at P_{O_2} values below P_{crit} (which is at maximum performance $\approx$0.5 mmHg) the O_2 consumption rate becomes P_{O_2} dependent and drops rapidly to 0 with falling P_{O_2}. In the present model in which only constant O_2 consumption rates are considered, this fact is taken account of by completely turning off O_2 consumption at P_{O_2} values below $P_{crit}/2$. The consequences of this simplified treatment of P_{O_2} dependence of the O_2 consumption rate have been assessed in a capillary domain cross section with a high O_2 consumption rate and low fiber P_{O_2}, in which case the largest effects are to be expected. To this end, local O_2 consumption rate has been assumed to depend on local P_{O_2} according to a Michaelis–Menten-type kinetics. O_2 reaction kinetics of the Michaelis–Menten type are parameterized by maximal $\dot{V}_{O_2}$ and the P_{O_2} at which half-maximal oxygen turnover occurs. The latter parameter was adjusted to yield 95% of maximum $\dot{V}_{O_2}$ at P_{crit}. For the choice of maximal $\dot{V}_{O_2}$ see below. Actual calculations were performed as follows: starting with a P_{O_2} profile for constant $\dot{V}_{O_2}$, a profile of local $\dot{V}_{O_2}$ was computed from the Michaelis–Menten kinetics. Vice versa, local P_{O_2} was determined by numerically integrating the radial P_{O_2} gradients that depend on local $\dot{V}_{O_2}$. This procedure was reiterated until stable P_{O_2} profiles resulted. The *average* O_2 consumption rate is an input parameter to the model. In comparing P_{O_2} profiles from models assuming constant and P_{O_2}-dependent local O_2 consumption rates, calculations from both models have to be based on the same input data and hence on the same *average* O_2 consumption rate. At the level of capillary domains, the average O_2 consumption rate is reflected in the transcapillary O_2 flux. Therefore, in performing the above computations for the model with P_{O_2}-dependent consumption rate one has to make sure that the transcapillary O_2 flux is the same as in the model employing constant consumption rate. This is achieved by adjusting maximum $\dot{V}_{O_2}$ (which is a parameter of the Michaelis–Menten kinetics) accordingly during the iteration.

10. Data

The data used in the computations are typical for working dog gracilis muscle and are compiled in Tables 1 and 2. Five O_2 consumption rates have been chosen, covering a range of ~20% to ~95% of maximum muscle performance of artificially stimulated muscles and corresponding to stimulation frequencies of 1, 2, 4, 6, and 8 Hz (Connett and Honig, 1989). Whereas in working muscle there is at least good qualitative agreement between model and experiment (Federspiel, 1986; Groebe and Thews, 1986, 1990b; Groebe 1990), the P_{O_2} drops between capillary and tissue predicted in resting muscle are only 1–2 mm Hg. This is at variance with Mb-O_2 saturation measurements that result in median values of P_{O_2} that are ~30 mm Hg below venous outflow P_{O_2} (C. R. Honig, deceased, personal communication, 1990). At present the cause for these discrepancies is unclear. Even though it is controversial if perfusion in working muscle is distributed more homogeneously than in resting muscle tissue (Laughlin, 1991), it is known that in the latter blood flow is intermittent and extremely heterogeneous: whereas red cell flux is present in some capillaries, stagnant RBC's are found in others, and the population of perfused capillaries changes with time (cf. Zweifach and Lipowsky, 1984). As a consequence, P_{O_2} distributions in resting muscle are most likely governed rather by temporal and spatial blood flow heterogeneities than by diffusive O_2 transport. Therefore, the range of O_2 consumption rates considered in this study has been restricted to working muscles.

Functional capillary densities have been estimated in accord with Honig and Odoroff (1981). Those authors found that, at a stimulation frequency of 4 Hz, more than twice as many capillaries are recruited, compared with a value of 510 mm^{-2} at rest. At 8 Hz, functional capillaries are derecruited to less than 1.5 times the resting fcd. Capillary length L of

TABLE 1 List of frequently used symbols and performance-independent data employed in the numerical evaluation. All data refer to 37°C

A	= Capillary domain cross sectional area	
α_{Blood}	= O_2 solubility in blood	= 1.4×10^{-6} mol ÷ ($l \times$ mm Hg)
α_{CFR}	= O_2 solubility in the carrier-free region	= 9.4×10^{-7} mol ÷ ($l \times$ mm Hg)
α_M	= O_2 solubility in the muscle fiber	= 9.4×10^{-7} mol ÷ ($l \times$ mm Hg)
α_{RBC}	= O_2 solubility in the RBC	= 1.5×10^{-6} mol ÷ ($l \times$ mm Hg)
$\mathscr{C}$, $\mathscr{C}(P)$	= Mean capillary blood O_2 content (at P_{O_2} P)	
$\mathscr{C}_A$	= Arterial blood O_2 content	
C_{Hb}	= Total Hb concentration in the RBC	= 0.0203 mol/l
C_{Mb}	= Total Mb concentration in the fiber	= 5.4×10^{-4} mol/l
d_{CFR}	= Thickness of carrier-free region	= 1.5 μm
D_{CFR}	= O_2 diffusion coefficient in the CFR	= 1.65×10^{-5} cm^2/s
D_M	= O_2 diffusion coefficient in the fiber	= 1.16×10^{-5} cm^2/s
D_{Mb}	= Mb diffusion coefficient in the fiber	= 5.47×10^{-7} cm^2/s
D_{RBC}	= O_2 diffusion coefficient in the RBC	= 9.5×10^{-6} cm^2/s
Hct	= Blood hematocrit	= 0.5
k	= Rate constant of O_2 dissociation from Hb-O_2	= 44 s^{-1}
K_{O_2}	= (Effective) O_2 conductivity	
L	= Capillary length	= 1150 μm
L_{RBC}	= Red cell length	= 5.2 μm
P, $\mathbf{P}(P^*)$	= Oxygen partial pressure (at effective P_{O_2} P^*)	
P^*, $\mathbf{P}^*(P)$	= Effective oxygen partial pressure (at P_{O_2} P)	
$\mathscr{P}(\mathscr{C})$	= Hb–O_2 equilibrium P_{O_2} at blood O_2 content $\mathscr{C}$	
P_{50}	= Half-saturation P_{O_2} of Mb	= 5.3 mm Hg
P_{crit}	= Critical mitochondrial P_{O_2}	= 0.5 mm Hg
φ	= Angular coordinate	
Φ_{RBC}	= RBC O_2 flux	
Φ_C	= Transcapillary O_2 flux	
$\dot{Q}_{Cap}$	= Mean capillary blood flow	
r	= Radial coordinate	
R_{CFR}	= Radius of carrier-free region	= 3.5 μm
R_{RBC}	= Red cell radius in capillaries	= 2.0 μm
S, $S(P)$	= Myoglobin O_2 saturation (at P_{O_2} P)	
$\mathscr{S}$, $\mathscr{S}(P)$	= Hemoglobin O_2 saturation (at P_{O_2} P)	
$\mathscr{S}_A$	= Arterial Hb–O_2 saturation	= 0.95
σ_{RBC}	= RBC surface area	= 65.3 μm^2
$\dot{V}_{O_2}$	= O_2 consumption rate of the muscle fiber	
V_{RBC}	= Red cell volume	= 66 fl
z	= Longitudinal coordinate	

1150 μm and blood Hb concentration of 163 g/l are from Gayeski and Honig (1988). Arterial O_2 saturation was set to 95%, and venous O_2 saturations were taken from Honig et al. (1984) and Honig and Odoroff (1981). Finally, blood flow rates were calculated to match arterial and venous saturations and O_2 consumption rates. The resulting values are well within the range of measured data (Honig and Odoroff, 1981).

Hemoglobin $\mathscr{P}_{50}$ and Hill coefficient n were taken from Clark et al. (1985) for 1–6 Hz. For near-maximal performance, there is considerable acidification of the blood, inducing a Bohr shift of the Hb oxygen dissociation curve (ODC), which raises P_{O_2} (e.g., to 26 mm Hg at a venous saturation of 42% and $\dot{V}_{O_2}$ = 14 ml O_2(100 g)$^{-1}$ min^{-1}; Honig and Odoroff, 1981) and which has to be accounted for. Therefore, $\mathscr{P}_{50}$ and n at 8 Hz were calculated by a least-squares fit of

TABLE 2 List of symbols (continued) and data specific for the respective stimulation frequencies studied

		Stimulation Frequency (Hz)					
		1	2	4	6	8	
$\dot{V}_{O_2}$	= Overall O_2 consumption rate	3	6	11	13	15	ml O_2/(100 g $\times$ min)
$\dot{Q}$	= Blood flow rate	26.1	40.2	68.6	84.1	123.5	ml/(100 g $\times$ min)
$\mathscr{S}_V$	= Venous Hb–O_2 saturation	0.45	0.30	0.25	0.275	0.42	
fcd	= Functional capillary density	800	950	1000	950	700	mm^{-2}
R_K	= Radius of capillary domain	19.9	18.3	17.8	18.3	21.3	μm
l_{RBC}	= Fraction of capillary length occupied by RBC's	0.444	0.5	0.571	0.625	0.667	
n	= Hill coefficient of Hb	2.65	2.65	2.65	2.65	3.58	
$\mathscr{P}_{50}$	= Half-saturation P_{O_2} of Hb	26.4	26.4	26.4	26.4	34.0	mm Hg

the first of Eqs. 2 to the Hb ODC for dog blood (Altman and Dittmer, 1972) that had been modified to match venous P_{O_2} and saturation. To take account of the fact that pH decreases gradually along the capillary, the P_{O_2} increments added to the above ODC were allowed to increase linearly with drop in O_2 saturation, starting at a value of 0 mm Hg (at arterial saturation) and ending at a value of 4.4 mm Hg (at venous saturation).

Other blood parameters are from Clark et al. (1985). The (large vessel or discharge) hematocrit *Hct* was computed as the ratio of Hb concentration in blood to Hb concentration in the RBC. Compared with O_2 binding to Hb, O_2 dissolved physically in blood is of minor importance. Therefore a homogeneous blood solubility α_{Blood} was assumed, which was calculated as hematocrit-weighted average of O_2 solubilities in RBC and in plasma (Zander, 1975). Intracapillary RBC length has been set to 5.2 μm, and intererythrocytic gap lengths of 1.25, 1.0, 0.75, 0.6, and 0.5 RBC lengths have been used for the five performances, respectively (in accord with unpublished data of C.R. Honig (deceased)). This choice of red cell spacings results in values for capillary hematocrit that are well below discharge hematocrit *Hct*. At a diameter of the capillary lumen of 5.3 μm (Eriksson and Myrhage, 1972), corresponding capillary hematocrits are 0.26 to 0.38 which are well within the range of observed values (Klitzman and Duling, 1979). RBC radius and surface were calculated to match L_{RBC} and V_{RBC}.

Further parameters, in particular the diffusivity of Mb in muscle cells, have been selected as discussed in Groebe and Thews (1990a), where the relevant references are also listed. For a discussion of uncertainties regarding myoglobin diffusivity in vivo see subsection 1 of the General Discussion.

RESULTS AND SPECIFIC DISCUSSION

P_{O_2} profiles at maximum muscle performance in planes defined by the capillary direction and by the bold lines in Fig. 4 for the triangular capillary domain and for a cylindrical capillary domain of same size are displayed in Fig. 5, left and right panels, respectively. Note that for technical reasons the abscissae in this figure have not been drawn to scale but are compressed in the longitudinal direction by approximately a factor of 10; thus, the longitudinal gradients compared with the radial ones appear ten times steeper than they really are.

Calculated P_{O_2} distributions are in good qualitative agreement with experimental results of Gayeski and Honig (1986, 1988) and with P_{O_2} profiles from a more complex mathematical model (Groebe 1990; see also the General Discussion section). At higher performances and remote from the capillary origin, profiles exhibit remarkably steep pericapillary P_{O_2} drops and shallow P_{O_2} gradients at low P_{O_2} levels in the rest of the fiber.

1. Adequacy of simplified procedure for treating O_2 release from the capillary

In formulating the basic model, a simplified description for O_2 release from the capillary was used, in which O_2 flux was restricted to locations adjacent to RBC's in the CFR and assumed uniform (with respect to the longitudinal coordinate) in the rest of the tissue. This overestimates P_{O_2} gradients in the carrier-free layer and underestimates them in tissue regions located next to capillaries. For cases in which this procedure might be an oversimplification, a more realistic approach was formulated in subsection 6 of the Analysis and Data section. This approach uses diffusing capacities that are

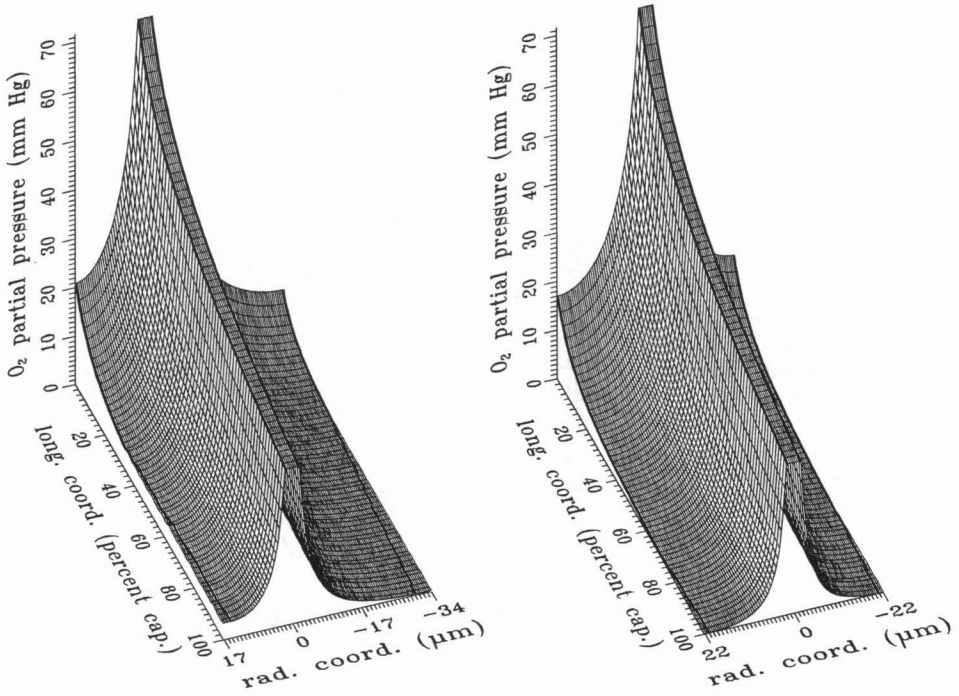

FIGURE 5 P_{O_2} profiles in planes defined by the capillary direction and by the bold lines in Fig. 4 for the triangular capillary domain (left) and for an axisymmetric cylindrical domain of same size (right) at near maximum performance. Within the capillary ($r \leq R_{RBC} = 2$ μm) mean red cell P_{O_2} is specified. Bold lines in the profiles delineate red cell surfaces ($r = R_{RBC}$) and boundaries of well-oxygenated tissue regions.

obtained from a solution of the two-dimensional time-dependent differential equation of red cell O_2 unloading under capillary conditions.

To test the simplified treatment of capillary O_2 release, P_{O_2} distributions for the five data sets in this study were calculated from both models and compared with one another. At the interface between CFR and fiber—where the largest errors are to be expected—P_{O_2} from the more realistic model was higher, in most cases by less than 1 mm Hg and in the most extreme case by 2 mm Hg. Further apart from the capillary, this difference distinctly decreased. Histograms from both models are very close, particularly for higher performances and lower values of P_{O_2}, so the simplified approach appears to be adequate under physiological conditions. This may be different in pathophysiological situations (e.g., severe anemia) if large intererythrocytic gaps are to be expected.

2. Adequacy of axially symmetric capillary domains at c/f ratios of up to 2

Fig. 5 contrasts P_{O_2} distributions for triangular (c/f ratio = 2, left) and cylindrical (c/f ratio = 1, right) capillary domains of same size, calculated in planes that are defined by the capillary direction and by the bold lines in Fig. 4, bottom and top panels, respectively. Note the asymmetry of the P_{O_2} distribution in the left panel (base of triangular domain to the left, corner to the right of capillary). The longer diffusion distances to the triangle's corner (right-hand side of the capillary) lead to a greater number of tissue sites with low values of P_{O_2} compared with those in the axially symmetric case (right panel). Fig. 6 gives the cumulative P_{O_2} histograms for the two capillary domains (△, triangular; ○, axially symmetric) at the five different performances considered. P_{O_2} deviations of the triangular from the axisymmetric case are much less pronounced in the histograms than could have been expected from the disparities in the shapes of capillary domains (Fig. 4, bottom panel) and from the differences between profiles in Fig. 5. This is because in the planes chosen for Fig. 5 deviations are the most extreme. Mean values and standard deviations of corresponding P_{O_2} probability distributions for the two cases differ by up to 5% but generally by less. As could have been expected from the shapes of the capillary domains, mean values are always larger and variation is smaller in the axially symmetric case. Major differences are found only at performances higher than the ones shown in Fig. 6, at which nonnegligible anoxia is present. In these cases, anoxia from the triangular model is significantly more pronounced.

In consequence, a c/f ratio of up to 2 generally does not lay any restrictions on the applicability of axisymmetric capillary cylinder models to muscle. Even at performances at which anoxia starts to occur, histograms from both type models as well as mean values and standard deviations are still very similar. However, the somewhat larger anoxic regions, which are revealed by the triangular model only, may be of physiological importance for $\dot{V}_{O_2}$ and $\dot{Q}$ regulation. It should be noted, though, that typical cell diameters in dog gracilis muscle are ~50 μm (Gayeski and Honig, 1986). This corresponds to capillary densities of 509 mm^{-2} at a c/f ratio of 1 and of 1018 mm^{-2} at a c/f ratio of 2. Although fcd of ~700 mm^{-2} is observed at maximum muscle performance in electrically stimulated muscles, fcd of ~1000 mm^{-2} is typical for stimulation at 4 Hz; i.e., in the most critical supply situations, c/f ratios are actually closer to 1 than to 2.

3. Role of O_2 diffusion parallel to capillary direction

Even more clearly than for circular and triangular capillary domains, the P_{O_2} histograms for the cases of combined radial and axial diffusion (not shown) and of exclusively radial

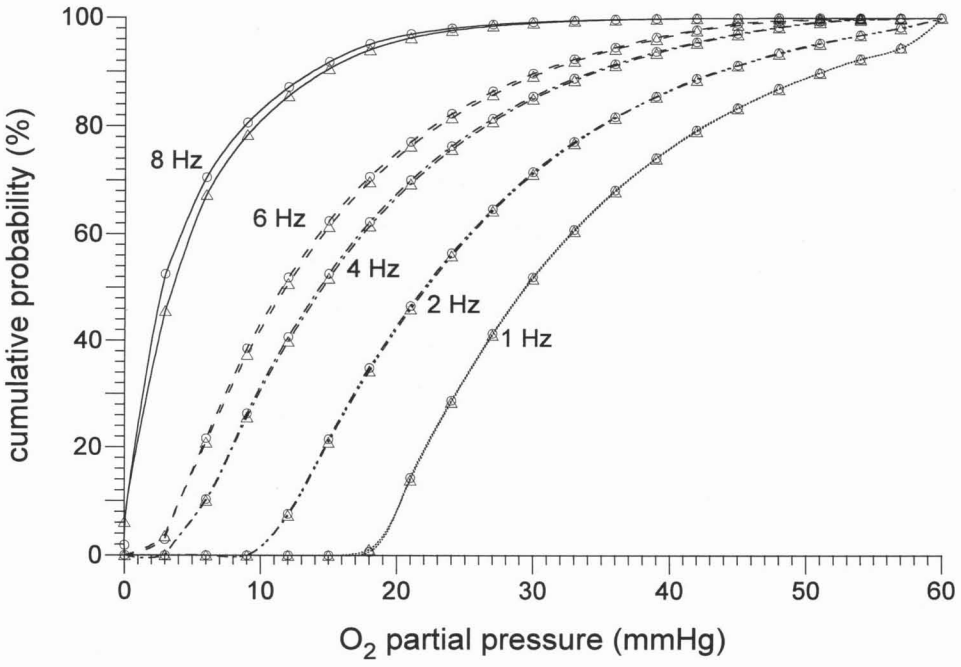

FIGURE 6 Cumulative P_{O_2} histograms for the triangular capillary domain (△) and for an axially symmetric capillary domain of same size (○) at the five different performances considered (cf. Table 2). Curve labels specify stimulation frequencies.

diffusion are virtually identical. The effect of diffusion parallel to the capillary direction on the distribution of P_{O_2} and transcapillary O_2 flux along the capillary is demonstrated in Fig. 7 for a muscle stimulated at 4 Hz (thin curves, exclusively radial diffusion; bold curves, combined radial and longitudinal diffusion). Graphs for other performances considered are similar. Solid curves refer to the left ordinate and give the P_{O_2} in the capillary (upper), at the interface between CFR and fiber (middle), and at the periphery of the capillary domain (lower tracing). Dashed curves show the transcapillary O_2 flux per u.l. of capillary, Φ_C (right ordinate). While without axial diffusion, Φ_C must be constant along the capillary, it turns out that this is also true over most of the capillary length if axial diffusion is considered. Yet Φ_C is distinctly higher near the capillary origin than along the rest of the capillary. This burst of oxygen is too small to change capillary P_{O_2} noticeably. Locally, however, it entails larger pericapillary P_{O_2} drops and lower tissue P_{O_2} readings by up to 6 mm Hg. Correspondingly, the maximum longitudinal gradients in the peripheries of capillary domains fall from 0.28 mm Hg/μm without axial diffusion to 0.12 mm Hg/μm if longitudinal diffusion is accounted for. For a muscle of similar O_2 consumption rate, Gayeski and Honig (1988) reported maximum longitudinal gradients of same magnitude. The average longitudinal P_{O_2} gradients from the model are even smaller than theirs. A remaining point of major inconsistency is their observation that "axial variability exhibits no orderly trend." Possible explanations are that measuring sites were not aligned exactly parallel to the capillary direction or that staggering of capillary origins (see, e.g., Lund et al., 1987) introduced some variability that is not accounted for in the model.

4. P_{O_2}-dependent O_2 consumption rate

Mitochondrial O_2 uptake is fairly independent of P_{O_2} unless P_{O_2} drops to very low values. Therefore, the effects of this P_{O_2} dependence on P_{O_2} distributions must be most pronounced in maximally working muscles near the venous capillary end where tissue P_{O_2} approaches zero. Radial P_{O_2} profiles for this situation are shown in Fig. 8 (dotted, constant $\dot{V}_{O_2}$; dashed, P_{O_2}-dependent $\dot{V}_{O_2}$, left ordinate) along with the local O_2 consumption rate $\dot{V}_{O_2}$ (solid, right ordinate). Interfaces between RBC, CFR, and muscle fiber are delineated by dotted vertical lines. While $\dot{V}_{O_2}$ is almost constant up to 15 μm into the fiber, it drops sharply at radial coordinates greater than that. Nevertheless, the two P_{O_2} profiles for constant and P_{O_2}-dependent $\dot{V}_{O_2}$ (dotted and dashed curves, left ordinate) are virtually indistinguishable. This is because at $r = 15$ μm, P_{O_2} and P_{O_2} gradients are already extremely small, so even massive (relative) changes in $\dot{V}_{O_2}$ and P_{O_2} gradients cannot noticeably alter the profile shape. It should be noted that maximum $\dot{V}_{O_2}$ for the P_{O_2}-dependent case was adjusted such that the *average* $\dot{V}_{O_2}$ equals the input $\dot{V}_{O_2}$ to the model; hence the transcapillary O_2 fluxes in both cases are the same.

In Fig. 8, the dependence of $\dot{V}_{O_2}$ on P_{O_2} is modeled by Michaelis–Menten-type kinetics, as this kinetics can well describe the experimentally observed relative constancy of $\dot{V}_{O_2}$ over a wide P_{O_2} range and the sharp drop in $\dot{V}_{O_2}$ at very low values of P_{O_2}. This is not meant to imply, however, that the chemical reactions taking place when O_2 is consumed in actual fact *are* of first order. Rather, it has been shown that $\dot{V}_{O_2}$ is related to the phosphorylation potential even at lower performance, which will have effects on the P_{O_2} dependence of $\dot{V}_{O_2}$ when oxygen becomes a limiting substrate (Connett and Honig, 1989; Connett et al., 1990).

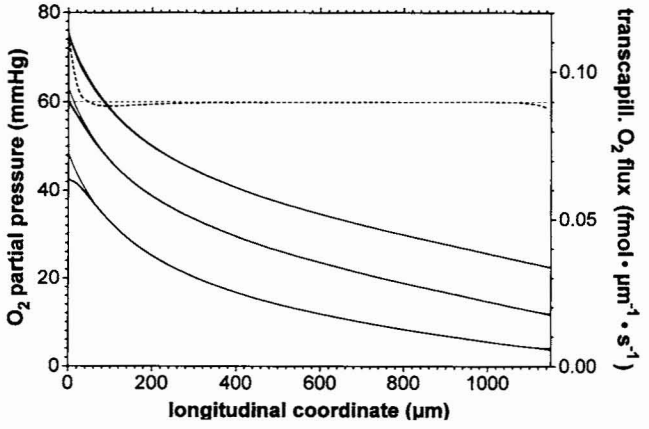

FIGURE 7 P_{O_2} and transcapillary O_2 flux along the capillary for a muscle stimulated at 4 Hz. Thin curves, exclusively radial diffusion; bold curves, combined radial and longitudinal diffusion. Solid curves refer to the left ordinate and give the P_{O_2} in the capillary (upper), at the interface between CFR and fiber (middle), and at the periphery of the capillary domain (lower). Dashed curves show the transcapillary O_2 flux per u.l. of capillary in units specified at the right ordinate.

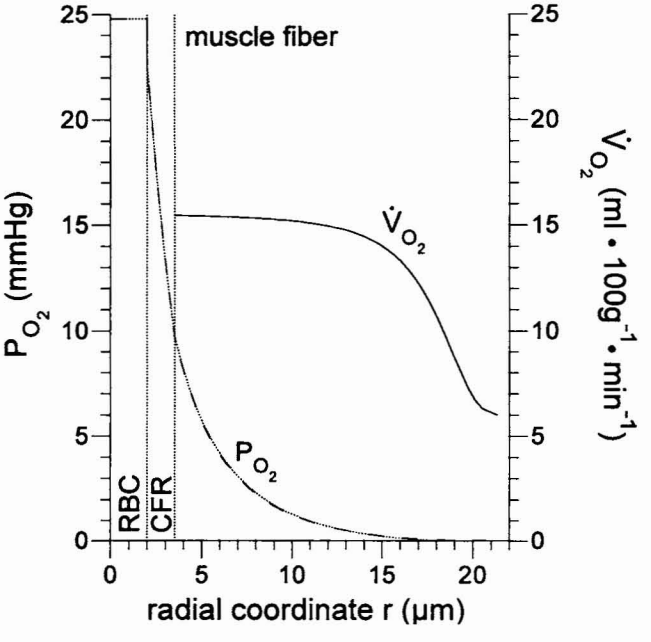

FIGURE 8 Comparison of radial P_{O_2} profiles for constant and P_{O_2}-dependent $\dot{V}_{O_2}$ (dotted and dashed curves, left ordinate). Interfaces between RBC, CFR, and muscle fiber are delineated by dotted vertical lines. Within RBC's, P_{O_2} pertinent to mean Hb–O_2 saturation is shown. The solid curve gives the local O_2 consumption rate $\dot{V}_{O_2}$ (right ordinate). While $\dot{V}_{O_2}$ is fairly constant up to 15 μm into the fiber, it sharply drops at radial coordinates greater than that. Nevertheless, the two P_{O_2} profiles are virtually indistinguishable.

5. Sensitivities of parameter dependencies of P_{O_2} distributions

In modeling, the input parameters to the model are always subject to errors. Except for random and systematic errors introduced by measurement, some of the required data are available only for muscles or even for species other than the one under consideration. Moreover, there are parameters that have not been measured systematically at all and may be estimated only from general physiological knowledge or from observations in samples of small sizes. Therefore, it is of interest to identify those parameters on which the resulting P_{O_2} distributions depend in a particularly sensitive fashion and for which more precise input data are needed.

5.1 Methodological considerations

When analyzing the individual dependencies it is essential to make sure that only the parameter under consideration is changed and that all others are kept constant. This requires identification of a set of parameters for which independent modification of each member is possible. When lowering venous saturation $\mathcal{S}_V$, for example, arterial saturation $\mathcal{S}_A$, blood Hb concentration $Hct\ C_{Hb}$, or perfusion rate $\dot{Q}$ will have to decrease, or O_2 consumption rate $\dot{V}_{O_2}$ must increase in order to maintain consistency. Therefore, only four of the five, $\mathcal{S}_A$, $\mathcal{S}_V$, $Hct\ C_{Hb}$, $\dot{Q}$, and $\dot{V}_{O_2}$, may be members of this parameter set. In actual experiments, $\mathcal{S}_A$, $\mathcal{S}_V$, $Hct\ C_{Hb}$, and $\dot{Q}$ are usually measured directly and $\dot{V}_{O_2}$ is calculated according to Fick's principle. Nevertheless, in the present investigation $\dot{V}_{O_2}$ and not $\dot{Q}$ has been made a member of the set of independent parameters because $\dot{V}_{O_2}$ characterizes the five performances under study, and therefore uncontrolled compensatory changes in $\dot{V}_{O_2}$ are not desirable. The members chosen for the set of independent parameters are listed in the legend of Fig. 9. All other parameters are dependent and may be calculated from the ones in the set.

It is the objective of this section to provide numerical data on the average change in tissue O_2 partial pressure, P_{O_2T}, associated with a given (small) error Δp in any of the input parameters p, which is given by

$$\overline{\Delta P_{O_2T}} = \overline{P_{O_2T}(\mathbf{x}, p + \Delta p) - P_{O_2T}(\mathbf{x}, p)} \approx \left[\overline{\frac{\partial P_{O_2T}(\mathbf{x}, p)}{\partial p}}\right]\Delta p,$$

where the overbar denotes the mean over all tissue

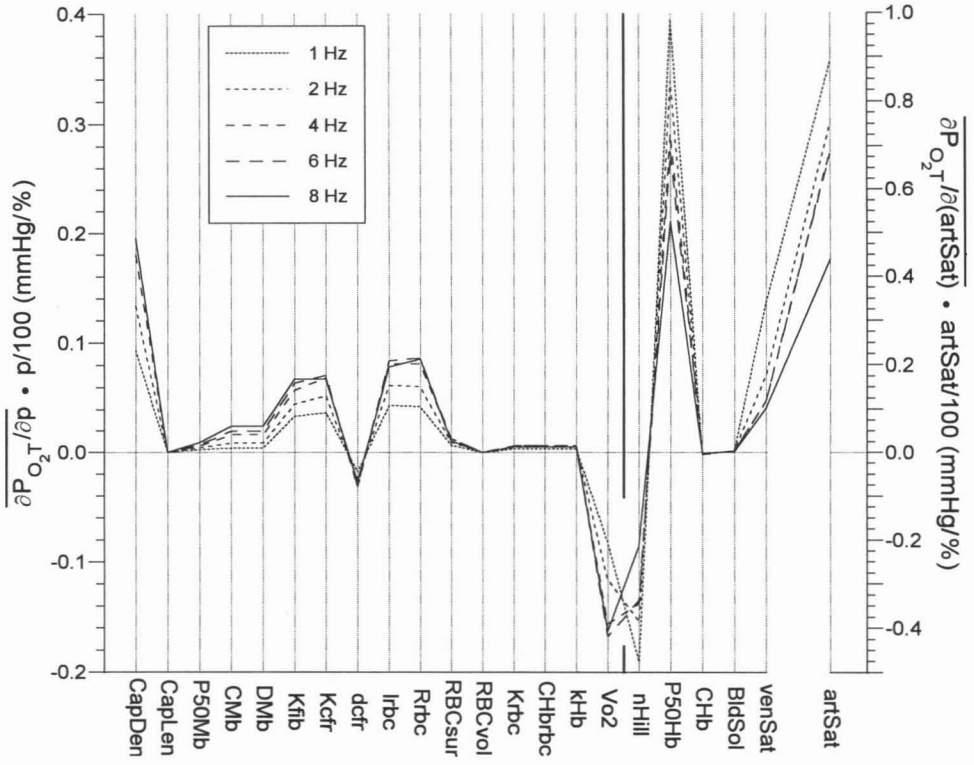

FIGURE 9 Parameter sensitivities of tissue P_{O_2}, $[\overline{\partial P_{O_2T}/\partial p}]\times(p/100)$ where p are the parameters specified in abbreviated form below the abscissa. Ordinate has been scaled to reflect P_{O_2T} changes (in millimeters of mercury) that are brought about by 1% errors in the respective parameters. Positive values indicate equidirectional changes of parameter p and P_{O_2T}; negative values imply that these changes are of opposite direction. At the right-hand side of the graph, there is a separate ordinate for the derivative with respect to arterial O_2 saturation (artSat), $[\overline{\partial P_{O_2T}/\partial \mathcal{S}_A}]\times(\mathcal{S}_A/100)$, because tissue P_{O_2} distributions are by far the most sensitive to $\mathcal{S}_A$. As specified in the in-figure legend, the dotted, dashed, and solid curves refer to the five stimulation frequencies considered (cf. Table 2). Individual parameters are abbreviated as follows and are explained in Tables 1 and 2: CapDen = fcd, CapLen = L, P50Mb = P_{50}, CMb = C_{Mb}, DMb = D_{Mb}, Kfib = $D_M\alpha_M$, Kcfr = $D_{CFR}\alpha_{CFR}$, dcfr = d_{CFR}, lrbc = l_{RBC}, Rrbc = R_{RBC}, RBCsur = σ_{RBC}, RBCvol = V_{RBC}, Krbc = $D_{RBC}\alpha_{RBC}$, CHbrbc = C_{Hb}, kHb = k, Vo2 = $\dot{V}_{O_2}$, nHill = n, P50Hb = $\mathcal{P}_{50}$, CHb = blood Hb concentration = $C_{Hb}\ Hct$, BldSol = α_{Blood}, venSat = $\mathcal{S}_V$, artSat = $\mathcal{S}_A$.

locations **x**; i.e., propagation of the error Δp into the resulting P_{O_2T}, is governed by the factor $[\partial P_{O_2T}/\partial p]$. Similarly, maximal error propagation and propagation into the means, $\overline{P_{O_2T}}$, and standard deviations, $\sigma(P_{O_2T})$, of tissue P_{O_2} probability distributions are governed by the partial derivatives $\max_{tissue}[\partial P_{O_2T}/\partial p]$, $\partial \overline{P_{O_2T}}/\partial p$, and $\partial \sigma(P_{O_2T})/\partial p$, respectively.

As can be seen from the model equations derived in the Analysis and Data section, tissue P_{O_2} depends on parameters in a highly nonlinear fashion. Therefore, the above first-order Taylor expansions may be expected to yield good approximations only for small increments Δp. On the other hand, uncertainties in the input data to O_2 supply models are often of considerable magnitude. To give an idea on how these larger errors in the input data corrupt the resulting P_{O_2} distributions, changes in mean tissue P_{O_2}, $\Delta \overline{P_{O_2T}}$, effected by a 50% increase and a 50% decrease in each of the parameters are also calculated.

In Fig. 9 results are presented graphically in the form of the mean changes in P_{O_2T}, $[\overline{\partial P_{O_2T}/\partial p}]\Delta p$, associated with given changes Δp in parameters p (which are specified in abbreviated form below the abscissa). Because the various parameters are of very different magnitude, the graphs are normalized to show P_{O_2} changes (in millimeters of mercury) for values of Δp that amount to +1% of the respective parameter values specified in Table 1 or 2. Positive values indicate equidirectional changes of parameter p and P_{O_2T}; negative values imply that these changes are of opposite direction. P_{O_2} changes for other (small) values of Δp may be estimated by multiplying the respective value from the graph by Δp (given in percent of p). At the right-hand side of the graph, there is a separate ordinate for the parameter p = arterial O_2 saturation (artSat) to which the tissue P_{O_2} distributions are by far the most sensitive. Parameter sensitivities of tissue P_{O_2} distributions depend largely on the actual physiological situation under study. To cover a physiological range, individual parameter sensitivities for each one of the five performances listed in Table 2 are given (dotted, dashed, and solid curves; see the in-figure legends). To facilitate comparison of the various graphs, the same mode of presentation and the same scaling of the ordinate have been chosen for displaying the effects on $\overline{P_{O_2T}}$ in the cases in which the actual changes in p were plus (Fig. 10) or minus 50% (Fig. 11) of the parameter values.

The corresponding graphs for $\partial \overline{P_{O_2T}}/\partial p$ and for $\max_{tissue}[\partial P_{O_2T}/\partial p]$ have not been displayed, as their appearance very much resembles the one for $[\overline{\partial P_{O_2T}/\partial p}]$. $\partial \overline{P_{O_2T}} \times \partial p$ is generally very close to $[\overline{\partial P_{O_2T}/\partial p}]$, whereas $\max_{tissue}[\partial P_{O_2T}/\partial p]$ is typically 1.5–3 times $[\overline{\partial P_{O_2T}/\partial p}]$. For p = arterial O_2 saturation, $\max_{tissue}$

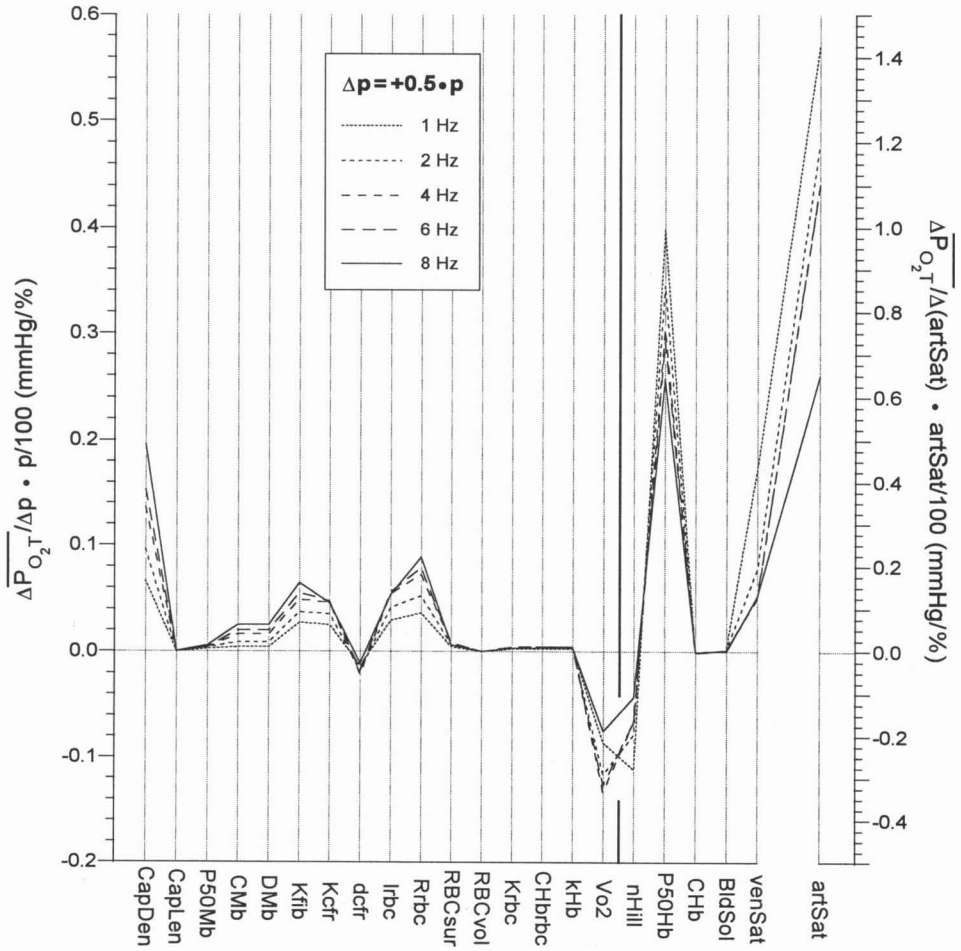

FIGURE 10 Changes in mean tissue P_{O_2}, $\overline{P_{O_2T}}$, per percent change in parameters p, brought about by 50% increases in p (i.e., the actual change in $\overline{P_{O_2T}}$ for a 50% parameter increase is 50 times the value displayed in the graph). Parameters p are specified in abbreviated form below the abscissa. The same conventions apply as in Fig. 9.

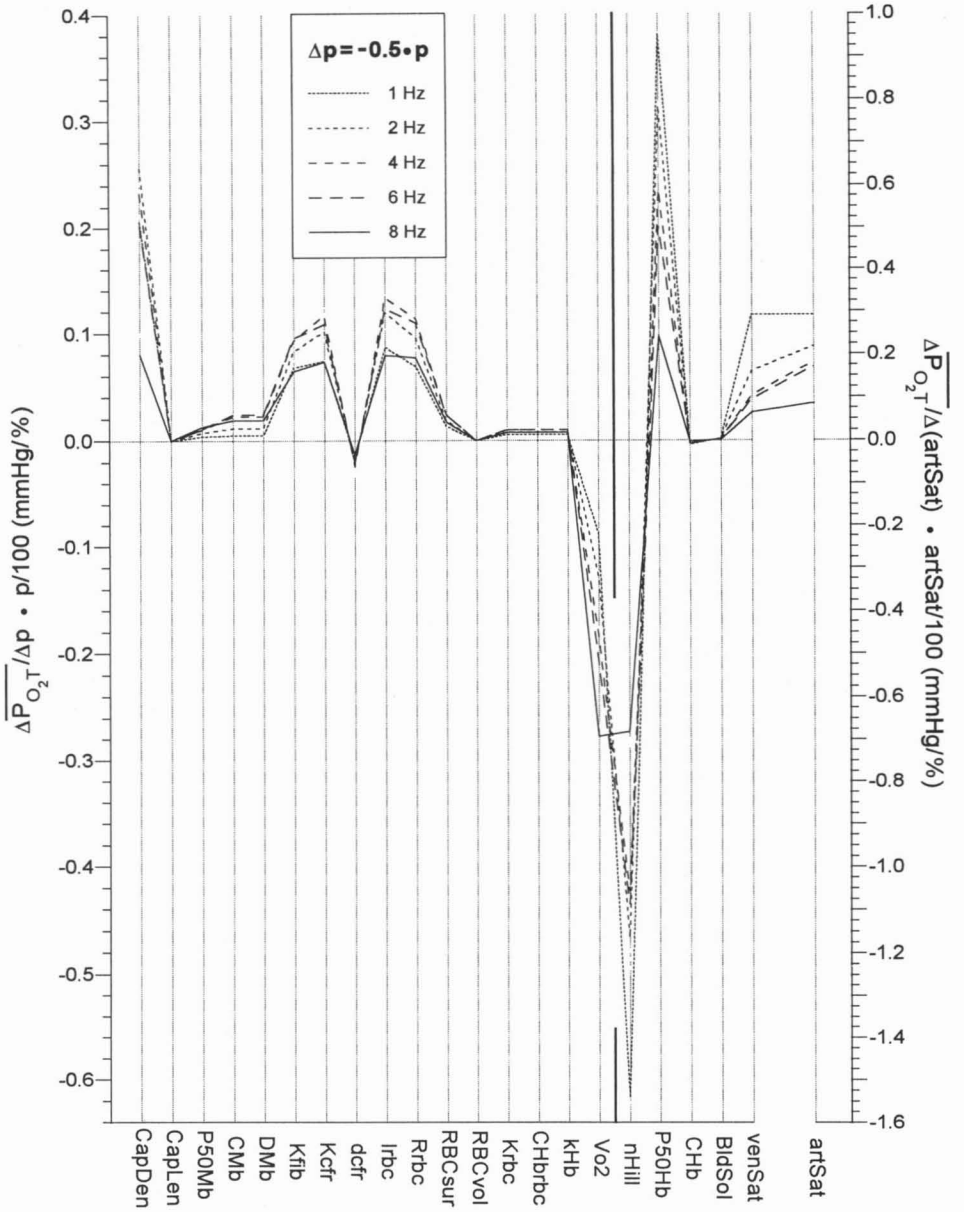

FIGURE 11 Changes in mean tissue P_{O_2}, $\overline{P_{O_2T}}$, per percent change in parameters p, brought about by 50% decreases in p (i.e., the actual change in $\overline{P_{O_2T}}$ for a 50% parameter decrease is -50 times the value displayed in the graph). Parameters p are specified in abbreviated form below the abscissa. The same conventions apply as in Fig. 9.

$[\partial P_{O_2T}/\partial p]$ is 5–8 times $\overline{[\partial P_{O_2T}/\partial p]}$. As interpretation of parameter dependencies is fairly complex, some introductory remarks may be suitable.

5.2 Determinants of muscle P_{O_2} distributions

Components of P_{O_2} drop. The drop in P_{O_2} between capillary origin and a given tissue location is the sum of two components: (i) the intravascular P_{O_2} drop between capillary origin and capillary sites near the tissue location in question (longitudinal P_{O_2} drop), which is a consequence of O_2 release along the capillary and which depends on arterial blood O_2 content, transcapillary O_2 flux Φ_C, capillary perfusion, and characteristics of O_2 binding in the blood, and (ii) the P_{O_2} drop between nearest capillary sites and tissue location (radial P_{O_2} drop), which is required as the driving force for O_2 diffusion out of the capillary into the tissue and which is governed by O_2 flux density (hence Φ_C) and diffusion-related material and geometric properties of the structures present along the O_2 diffusion path.

Accordingly, a parameter may influence P_{O_2T} by one of two mechanisms: either it changes mean capillary P_{O_2}, bringing about parallel changes in P_{O_2T} (as n, $\mathcal{P}_{50}$, blood Hb concentration, $\mathcal{S}_A$, $\mathcal{S}_V$, or $\dot{Q}$ does), or it increases/decreases O_2 flux density or O_2 diffusional resistance somewhere in the radial O_2 diffusion path and by so doing increases/decreases radial P_{O_2} gradients and lowers/raises P_{O_2T} (as fcd, P_{50}, C_{Mb}, D_{Mb}, $D_M\alpha_M$, $D_{CFR}\alpha_{CFR}$, d_{CFR}, l_{RBC}, R_{RBC}, σ_{RBC}, $D_{RBC}\alpha_{RBC}$, or C_{Hb} does).

Radial P_{O_2} gradients and O_2 flux density. Radial gradients maintain diffusional O_2 flux from RBC to tissue. P_{O_2} gradients are equal to O_2 flux density (the O_2 flux per unit area normal to the direction of the flux) divided by the (effective) O_2 conductivity K_{O_2} (which is defined and discussed in and near Eq. 8 and is graphed in Fig. 2). As a consequence, P_{O_2} gradients are steepest where O_2 flux density is largest and

K_{O_2} is smallest. In the intracapillary and pericapillary regions, the cross-sectional area over which the O_2 flux is distributed ("surface effective in O_2 exchange") is minimal; yet all the O_2 supplying the fiber has to pass through it. Therefore, O_2 flux densities are highest here. Furthermore, $\dot{V}_{O_2}$ is small (carrier not present or inefficient because of high P_{O_2}; cf. Fig. 2). As a joint effect, intracapillary and pericapillary P_{O_2} gradients are steepest, and the entire tissue P_{O_2} profile is dominated largely by the P_{O_2} drops in and near capillaries.

5.3 Interpretation of parameter dependencies of P_{O_2T}

In the following, the individual parameter dependencies from Fig. 9 are examined with respect to their underlying operating mechanisms and to their importance.

Parameters affecting longitudinal P_{O_2}. (See Fig. 9, parameters to the right of the bold vertical line.) As mentioned above, maximum values of $[\partial P_{O_2T}/\partial p]$ are attained for p = artSat. Mediated by the same mechanism, the effects of errors in the Hb oxygen dissociation curve—which is parameterized by hemoglobin $\mathcal{P}_{50}$ (P50Hb) and Hill coefficient n (nHill)—are among the most severe ones. Venous saturation, $\mathcal{S}_V$ (venSat) acts upon mean capillary P_{O_2} and therefore has effects similar to, though smaller than, those of $\mathcal{S}_A$, $\mathcal{P}_{50}$, and n. Blood hemoglobin concentration (CHb) and whole blood physical O_2 solubility (BldSol) do not produce any effects at all if the other parameters—in particular $\mathcal{S}_V$—are kept constant by adapting perfusion rate accordingly (see below).

Parameters affecting radial P_{O_2} drop. (See Fig. 9, parameters to the left of the bold vertical line.) The importance of functional capillary density fcd (CapDen) and oxygen consumption rate $\dot{V}_{O_2}$ (Vo2) is explained by the fact that radial P_{O_2} drops are—in the absence of facilitation—proportional to transcapillary O_2 flux and hence proportional to $\dot{V}_{O_2}$ and inversely proportional to fcd. To understand the effects of RBC radius, R_{RBC} (Rrbc), fraction of capillary length occupied by RBC's, l_{RBC} (lrbc), and O_2 conductivities of CFR and muscle fiber, $D_{CFR}\alpha_{CFR}$ (Kcfr) and $D_M\alpha_M$ (Kfib), one has to recall that P_{O_2} gradients are steepest in the pericapillary region (small surface effective in O_2 exchange, high O_2 flux density, small (effective) K_{O_2}). As a consequence, pericapillary P_{O_2} drops and P_{O_2T} depend rather sensitively on any parameter that affects the surface effective in O_2 exchange between RBC's and muscle fiber (such as R_{RBC} and l_{RBC}; cf. Groebe and Thews, 1989, 1990b) or on diffusion-related material properties in the (peri)capillary region (such as $D_{CFR}\alpha_{CFR}$). Moreover, in fiber portions located next to the CFR, P_{O_2} is high and Mb is close to fully saturated and thus not functional as an O_2 carrier ("region deficient of functional carrier"; cf. Groebe 1990). Therefore, O_2 transport takes place mainly by free O_2 diffusion with the consequences that effective K_{O_2} is close to free O_2 conductivity $D_M\alpha_M$ and that $D_M\alpha_M$ has significance similar to that of $D_{CFR}\alpha_{CFR}$.

The latter observation also explains the otherwise surprising finding that P_{O_2T} is only slightly sensitive to the thickness of the CFR (dcfr): A thicker carrier-free region entails a lower K_{O_2} at the interface between CFR and fiber and thus is partly compensated for by a thinning of the region deficient of functional carrier—and vice versa.

Compared with muscle fiber free O_2 conductivity $D_M\alpha_M$, tissue P_{O_2} is at least three times less sensitive to the parameters governing Mb-facilitated O_2 diffusion, which are Mb concentration (CMb), Mb diffusivity (DMb), and Mb P_{50} (P50Mb). This is true even at maximum performance, in which the bulk of the fiber exhibits low P_{O_2} and facilitated transport may exceed free O_2 transport by more than five-fold (cf. Fig. 2). Because in most of the capillary domain free O_2 diffusion accounts for merely a small fraction of total O_2 diffusive flux, one might have expected the opposite to hold true. This apparent contradiction is once again a consequence of the mentioned pericapillary region in which Mb is very little functional as an O_2 carrier and in which P_{O_2} gradients are steep. Therefore, the P_{O_2} drops across this region more strongly determine P_{O_2T} than gradients further remote from the capillary. The conductivity within the region deficient of functional carrier, however, is close to free O_2 conductivity and largely independent of Mb parameters. This explanation must not be misinterpreted in a sense that Mb-facilitated O_2 diffusion is not important in red muscle. Rather, at low P_{O_2}, diffusion of Mb-O_2 allows for large O_2 fluxes in the absence of significant P_{O_2} gradients by that supplying O_2 to regions that otherwise would become anoxic. Hence, changes in Mb parameters may drastically change the extent of tissue anoxia but still have comparatively little influence on P_{O_2} distributions.

RBC surface area (RBCsur), RBC volume (RBCvol), intracellular hemoglobin concentration (CHbrbc), and Hb-O_2 reaction kinetics (kHb) have very little effect because they affect only the P_{O_2} drop within the RBC, which in any case represents but a small portion of total radial P_{O_2} drop. Therefore, even considerable errors in these parameters turn out to be insignificant.

Capillary length L, blood Hb concentration Hct C_{Hb}, and O_2 consumption rate $\dot{V}_{O_2}$. Note from Fig. 9 that tissue P_{O_2} is independent of capillary length (CapLen). This may appear to be peculiar; it is, however, merely a consequence of our (natural) choice of input data: Clearly, the volume of tissue supplied by one individual capillary is proportional to capillary length L. Given the volume-related perfusion rate $\dot{Q}$, blood flow in this capillary therefore also needs to be proportional to L. As one can easily show, this results in probability distributions of the tissue P_{O_2} that are independent of L. This has the agreeable consequence that—if axial diffusion is negligible—knowledge of capillary length (or more precisely of red cell flow path length, which may be hard to measure under certain circumstances) is not required for calculating radial P_{O_2} profiles and tissue P_{O_2} histograms.

As in the case of capillary length it may be surprising that the effects of $\dot{V}_{O_2}$ and *Hct* C_{Hb} are rather small or even absent. This is also a consequence of our choice of a set of independent parameters in which $\mathcal{S}_A$, $\mathcal{S}_V$, $\dot{V}_{O_2}$, and not $\dot{Q}$ were included. Therefore, a decrease in *Hct* C_{Hb} at constant $\mathcal{S}_A$ and $\mathcal{S}_V$ is compensated for by comparable increase in $\dot{Q}$, keeping capillary P_{O_2} at each longitudinal position constant. For the

same reason, a change in $\dot{V}_{O_2}$ affects only radial and not longitudinal P_{O_2} drops. If changes in longitudinal gradients were allowed by keeping $\dot{Q}$ instead of $\mathcal{S}_V$ constant, sensitivities of 0.22–0.31 mm Hg/% for $\dot{V}_{O_2}$ and of 0.06–0.14 mm Hg/% for *Hct* C_{Hb} would result.

5.4 Effect of performance on parameter dependencies of P_{O_2T}

It is quite interesting to note that (i) the sensitivity to any parameter that changes mean capillary P_{O_2} (such as n, $\mathcal{P}_{50}$, $\mathcal{S}_V$, and $\mathcal{S}_A$) is larger at low performance than at high performance, whereas (ii) this relation is (roughly) reversed for parameters that exert influence on radial P_{O_2} drops (such as fcd, P_{50}, C_{Mb}, D_{Mb}, $D_M\alpha_M$, $D_{CFR}\alpha_{CFR}$, d_{CFR}, l_{RBC}, R_{RBC}, σ_{RBC}, $D_{RBC}\alpha_{RBC}$, C_{Hb}, k, and $\dot{V}$). These two observations may be explained as follows:

(i) Mb-facilitated O_2 diffusion is P_{O_2} dependent, as shown in Fig. 2. Its importance relative to free O_2 diffusion is the greater (and changes the more rapidly with P_{O_2}) the lower the tissue P_{O_2}, hence the higher performance (cf., e.g., Fig. 6). Therefore, at low performance (P_{O_2T} being high) facilitation is small and fairly independent of P_{O_2}. In this case, the entire distribution of P_{O_2T} shifts up and down in parallel with capillary P_{O_2}. At rising performance, growing fractions of tissue are at low P_{O_2}, which changes the situation: An increase in capillary P_{O_2} may well raise P_{O_2} in the pericapillary region, but this has the consequence that facilitation and effective O_2 conductivity fall; hence steeper P_{O_2} gradients are required to maintain a constant O_2 flux. In other words, part of the gain in capillary P_{O_2} is "eaten up" by steeper drops in driving force, which are necessary because of the lower effective conductivity associated with higher P_{O_2}. Only part of the increase in capillary P_{O_2} is passed on to the bulk of the tissue outside the pericapillary region—which, by the way, partly explains why Gayeski and Honig (1988) were unable to demonstrate longitudinal P_{O_2} gradients in tissue, which were associated with capillaries. This latter portion of the intracapillary gain in P_{O_2} becomes smaller at lower P_{O_2} (i.e., at higher performance) because effective O_2 conductivity falls the more rapidly with increasing P_{O_2} the lower the actual P_{O_2} level. In consequence, mean tissue P_{O_2} tends to turn more and more insensitive to capillary P_{O_2} with increasing performance.

(ii) The magnitude of intracapillary and pericapillary P_{O_2} drops is proportional to the transcapillary O_2 flux Φ_C. Therefore, whatever effect a parameter change may have on the radial intracapillary or pericapillary P_{O_2} drops, the magnitude of this effect is always weighted by Φ_C at the respective performance. As Φ_C goes up with performance the magnitude of the effect of a given parameter change will also increase, which by definition implies an increase in sensitivity. However, this increase in sensitivity is partly counteracted by the loss in sensitivity of P_{O_2T} to capillary (and also to pericapillary) P_{O_2} discussed in point (i). This is why for some parameters sensitivity becomes less again at highest performance.

5.5 Effects of large changes in parameters on mean tissue P_{O_2}, $\overline{P_{O_2T}}$

Figs. 10 and 11 give the difference quotients ($\Delta\overline{P_{O_2T}}\Delta p$) ($p$/100) for changes in the parameters p of plus or minus 50%, respectively. For the parameter artSat, a 50% increase is not feasible, and $\mathcal{S}_A = 0.99$ has been used instead. To facilitate comparison with Fig. 9, the same mode of presentation (change in $\overline{P_{O_2T}}$% increase in parameter p) and the same scaling of the ordinate have been chosen. Compared with that in Fig. 9, the common pattern of the $\Delta\overline{P_{O_2T}}\Delta p$ values in Figs. 10 and 11 is obviously the same, and differences are found only in their relative magnitudes. When the effects of a 50% increase are compared with those of a small parameter change, $\Delta\overline{P_{O_2T}}\Delta p$ quite generally is larger for parameters affecting longitudinal P_{O_2} drop and smaller for those affecting radial P_{O_2} drop—and the reverse holds true for a 50% parameter decrease.

5.6 Parameter dependencies of $\sigma(P_{O_2T})$

From the studies of Gayeski and Honig (1986, 1988) it may be concluded that heterogeneities in tissue P_{O_2} arise primarily from interregional differences in the O_2 supply conditions. Heterogeneities within individual capillary domains appear to be of subordinate importance. Therefore, parameter dependencies of $\sigma(P_{O_2T})$ are discussed very briefly.

With few exceptions, the sensitivities of $\sigma(P_{O_2T})$ exhibit a pattern similar to that of P_{O_2T}, i.e., large increases of P_{O_2T} with some parameter correspond to large increases in heterogeneity. Moreover, for most parameters the effects of performance on sensitivities are retained. In particular, changes in most of the parameters acting on radial intracapillary and pericapillary P_{O_2} drops (such as fcd, $D_M\alpha_M$, $D_{CFR}\alpha_{CFR}$, d_{CFR}, l_{RBC}, R_{RBC}, σ_{RBC}, and $D_{RBC}\alpha_{RBC}$) modify $\sigma(P_{O_2T})$ in the same fashion as they modify P_{O_2T}. This is a consequence of P_{O_2} dependence of Mb-facilitated O_2 diffusion (which was detailed in subsection 5.4, point (i)): falling pericapillary P_{O_2} drops result in rising P_{O_2T}, rendering facilitation less efficient. Consequently, for a given O_2 flux, steeper radial gradients along the rest of the diffusion path (outside the pericapillary region) are required which increases radial heterogeneity. On the other hand, at higher performances, larger Mb concentration and diffusivity or lower Mb P_{50} render facilitation more efficient and enhance radial homogeneity. For reasons explained above, however, the latter effects are small. Heterogeneity in muscles stimulated at 1 Hz is virtually unchanged by parameters mentioned so far, which nicely demonstrates the relations between Mb facilitation of O_2 diffusion and P_{O_2} discussed in subsection 5.4, point (i).

For increasing arterial O_2 saturation, increasing hemoglobin $\mathcal{P}_{50}$, and decreasing Hill coefficient, both mean capillary P_{O_2} (hence radial P_{O_2} variations) and longitudinal P_{O_2} variations increase. Therefore, the overall heterogeneity in P_{O_2T} must increase also.

GENERAL DISCUSSION

The model presented in this study is much simpler than the ones used in our preceding papers (Groebe, 1990; Groebe and Thews, 1990a, 1990b). Concentrating on just one capillary and neglecting diffusional capillary interactions allow one to include red cell O_2 unloading along the capillary and P_{O_2}-dependent facilitation of O_2 diffusion by Mb with comparatively little effort. Based on the results of former investigations (Hellums, 1977; Groebe and Thews, 1989, 1990a), it was possible to take account of intracapillary plasma gaps interspersed between red cells without considering axial diffusion explicitly. The moderate complexity of the present model offers the additional advantages that it may be programmed easily and that its requirements in computer time are low. For the latter reason, it can be used for calculation of parameter sensitivities in which large numbers of program runs need to be performed or for statistical evaluations (e.g., when studying the joint effects of heterogeneities in, say, the size of capillary domains and in capillary blood flow rates). Because the model does not consider diffusive interactions between adjacent capillary domains, only large-scale heterogeneities (i.e., heterogeneities that are not partly compensated for by O_2 diffusion from better- to worse-supplied capillary domains) can be assessed. To that end, the model is to be run multiply with different settings for the input parameters, which are taken from a discretized joint probability distribution of the parameters under study. Weighting the P_{O_2} probability distribution that results in each model run with the probability of the respective parameter vector and accumulating the weighted P_{O_2} distributions over all model runs give an approximation to the P_{O_2} distribution in heterogeneous tissue.

As a further advantage, the transparency of this model allows one to assess the adequacy of concepts such as CFR or carrier deficient region for explaining experimentally observed characteristics of muscle P_{O_2} distributions without having to worry that the results might be joint effects of a large number of features included in the model. In this way, concepts for understanding the underlying mechanisms may be developed and questions may be formed that then may need to be answered with the use of more complex models (e.g., the one of Groebe 1990). The disadvantage of this approach is that a number of simplifying assumptions had to be made that need to be justified.

1. Deficiencies of the model

Capillary cylinder models generally assume that the tissue contains parallel straight capillaries and that each of them supplies a well-defined capillary domain (in which diffusion along the capillary direction is negligible). The assumption of parallel straight capillaries is satisfied reasonably well in muscle. While in the (most extreme) example of triangular capillary domains it has been shown that the precise shape of domains is not of major importance for the results (see subsection 2 in the Results and Specific Discussion section), it is not clear at all that capillary domains are *a priori* well defined. Temporal and spatial blood flow heterogeneities in adjacent capillaries, staggering of capillary origins, capillary branching, or diffusional O_2 transport from well to poorly supplied regions all may modify capillary domain cross-sectional area along the capillary and/or with time. This is a problem that cannot conclusively be settled here but needs to be assessed by a more complex model that allows for a number of capillaries with arbitrary capillary geometries and flows. At present there is no lack of such models, even for myoglobin containing tissue (e.g., Hoofd et al., 1989; Groebe, 1990). The problem is rather how to choose realistic sets of input data inasmuch as to date measurements of joint parameter distributions, most importantly for capillary geometries and blood flows, are not available. Although the consequences of an a priori definition of capillary domains cannot be assessed here, there is evidence that the present approach is not too far off the line: (i) Results agree qualitatively with measured data (Gayeski and Honig, 1986, 1988) and (ii) with predictions for P_{O_2} distributions from more complex models (Federspiel, 1986; Groebe, 1990; Groebe and Thews, 1990a, 1990b). (iii) First attempts to relate P_{O_2} histograms measured in individual muscles quantitatively to modeling results calculated on the basis of input data that are specific for these very same muscles are quite encouraging. (iv) Despite the presence of myoglobin, diffusive transport of oxygen over long distances—and this includes even the adjacent capillary domains—is not very effective. If, e.g., an additional O_2 flux of 25% of the "regular" transcapillary flux were to be transported out of a capillary with 25% higher capillary blood flow (so longitudinal P_{O_2} drops remain unchanged) over a distance of $1.5 \times R_K$ (R_K is the radius of capillary domain), P_{O_2} at $1.5 \times R_K$ would fall to 0 mm Hg after 87% or 20% of the capillary length at 4 or 8 Hz stimulation rate, respectively. If capillary blood flow were not adapted to the increased O_2 demand these percentages would be 70% or 16% of the capillary length, respectively. This means that, toward the venous capillary end where compensation of anoxia would be needed the most, capillary P_{O_2} is not high enough to support even the moderate additional O_2 flux assumed here. These results would even be much less favorable for long-range diffusion if axial symmetry had not been assumed.

In subsection 3 of the Results and Specific Discussion section, it has been shown that axial diffusion has virtually no effect on P_{O_2} histograms and may safely be neglected. According to Fig. 5, considerable P_{O_2} gradients parallel to the capillary appear to be present within the tissue cylinder, particularly near the capillary origin. These apparent gradients are due to the fact that Fig. 5 has not been drawn to scale but is compressed in the longitudinal direction by a factor of ~10. Longitudinal gradients from the axial diffusion model are indeed small, and their magnitude is in agreement with experimental findings (Gayeski and Honig, 1988).

In model formulation it has been assumed that within the CFR O_2 diffusion is exclusively radial and takes place adjacent to erythrocytes only. Within the tissue, radial O_2 flux was taken to be homogeneous, with no differences in O_2 flux

between locations next to RBC-containing capillary sites and next to plasma gaps. By this simplification one overestimates P_{O_2} gradients in the CFR and underestimates P_{O_2} gradients in the muscle cell near capillaries. Moreover, steady-state conditions are assumed in a vicinity of the capillary. In subsection 1 of the Results and Specific Discussion section, this was shown to be a good approximation under conditions prevailing in working muscle. In case this should be required, the above-mentioned simplified treatment of O_2 release from the capillary may be replaced by a more realistic one employing RBC/capillary diffusing capacities (subsection 6 of the Analysis and Data section).

Assuming a constant O_2 consumption rate throughout the capillary domain and no O_2 consumption wherever P_{O_2} falls below a value of $P_{crit}/2 = 0.25$ mm Hg does not practically change the resulting P_{O_2} profiles at all compared with the case of P_{O_2}-dependent $\dot{V}_{O_2}$ (subsection 4 of the Results and Specific Discussion section). Further simplifying assumptions were shown earlier not to introduce major errors in the results (Groebe, 1990).

Recently, evidence has been put forth that the myoglobin diffusivity chosen for the present calculations (cf. Groebe and Thews, 1990a) may be too large by a factor of 4–5 (Baylor and Pape, 1988; Jürgens et al., 1994). The experimental methods used in these studies are all based on direct (photometric) observation of the disappearance of an artificially produced bolus of met-Mb owing to Mb diffusion in the muscle fiber. Even though this approach appears to be very elegant and straightforward, the actual techniques are still far from being beyond question:

In Baylor and Pape (1988) a met-Mb bolus was injected into a muscle fiber at a concentration that is more than 20 times the one in dog gracilis muscle and is not much less than total protein concentration in native muscle. By this, (i) Mb diffusion must have been slowed down considerably and (ii) large changes in protein concentration (and in D_{Mb}) along the fiber must have existed that should have been but were not considered when the met-Mb concentration profiles were evaluated for D_{Mb}.

In Jürgens et al. (1994) myoglobin naturally present in rat diaphragm muscle fibers was converted to met-Mb by a brief high-energy pulse of UV irradiation. D_{Mb} has been calculated from the decay of the met-Mb signal in the center of the irradiated field and the initial met-Mb concentration distribution along the fiber. Immediately following the UV pulse, there is an apparently irreversible decay in absorbance of unknown origin that is independent of met-Mb formation, the time constant of which is ~50 s and that is corrected for by the authors. Nevertheless, this change in tissue absorbance suggests the presence of some slower process of tissue degradation involving, e.g., chemicals such as oxidants that were synthesized under the influence of UV irradiation. Oxidants, on the other hand, may give rise to continuing met-Mb formation, which would mask disappearance of met-Mb by diffusion and which thus would decrease apparent D_{Mb}.

The intracellular net charge of Mb is close to zero (or slightly negative; I.P. = 7.0), and practically no electrical interactions between Mb and the negatively charged fiber proteins are to be expected. However, Baylor and Pape (1988) as well as Jürgens et al. (1994) used met-Mb for which adsorption to the muscle proteins might be different from the one of Mb owing to its additional positive charge. This would also render $D_{met\text{-}Mb}$ different from D_{Mb}.

Further conceivable reasons for systematic errors in both methods include uncertainties in the initial distribution of met-Mb along the fiber, inaccuracies in the determination of the rate of met-Mb reduction by met-Mb reductase, or treatment of the latter process as a first-order reaction, which might be an oversimplification.

Finally, in both studies only diffusivities *along* the fiber have been assessed and not the ones *perpendicular* to the fiber direction, which are the relevant ones for Mb facilitation of O_2 transport. Even though one would intuitively expect transversal diffusivities to be smaller than longitudinal ones, this might not hold true: e.g., the *Z* lines might be very slightly permeable to the Mb molecule, so Mb would be "compartmented" in thin slabs of muscle fiber (cf. Baylor and Pape, 1988).

For all of these reasons, for the time being, the "classical" data are used. If, however, Mb diffusivities should turn out to be substantially lower than presently thought, radically new concepts would be needed to reconcile experimental P_{O_2} profiles (Gayeski and Honig 1986, 1988) and theoretical predictions (Federspiel 1986, Groebe 1990, 1992, Groebe and Thews 1990b).

2. Relation to former work

Good qualitative agreement with experimental findings and with other modeling results has been mentioned above. The relation of the present investigation to the work of a number of other researchers (in particular of Federspiel, 1986) is the same as that of Groebe (1990) and has been discussed there.

To allow for a more specific discussion of relations between different models, results from the present model, from Groebe (1990) and from Groebe and Thews (1990b) have been compared. This comparison is based on similar data sets, all of which represent muscles at near maximal performance and which are detailed in the cited articles. Fig. 12 displays radial P_{O_2} distributions from the three models for different values of capillary P_{O_2}, corresponding to locations near the capillary origin, halfway down the capillary, and near the venous capillary end (solid curves, present model for stimulation rate 8 Hz; dashed curves, selected profiles from Fig. 6 of Groebe (1990), with capillary P_{O_2} values matching the ones from the present model; dotted curves, profiles along radial tracks, obtained from the graphs in Figs. 2 and 4 of Groebe and Thews (1990b)). Interfaces between RBC, CFR, and muscle fiber are delineated by dotted vertical lines. Within RBC's, P_{O_2} pertinent to mean Hb-O_2 saturation is shown. Care was taken to make sure that all profiles were

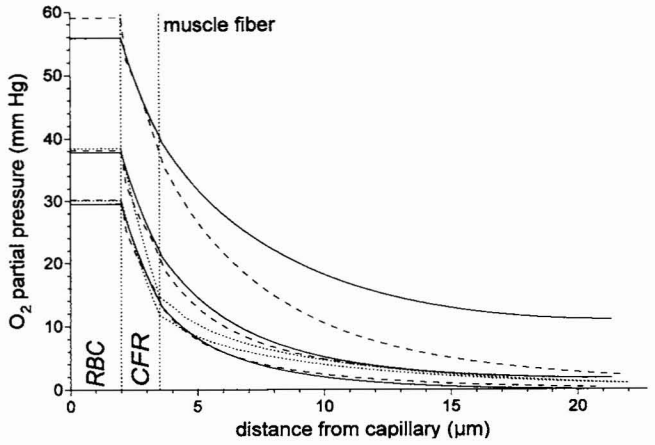

FIGURE 12 Comparison of radial P_{O_2} profiles from three models for muscles at near maximal performance and for different values of capillary P_{O_2}. Solid curves, present model; dashed curves, Groebe (1990); dotted curves, Groebe and Thews (1990b). Interfaces between RBC, CFR, and muscle fiber are delineated by dotted vertical lines. Within RBC's, P_{O_2} pertinent to mean Hb–O_2 saturation is shown.

determined along lines running perpendicular to the capillary direction and connecting the centers of an erythrocyte and a muscle fiber. The three studies represent grossly different mathematical approaches to modeling O_2 transport in tissue. Nevertheless, there is remarkable agreement between corresponding profiles. Compared with the profiles from the present study, the dotted midcapillary profile (Groebe and Thews, 1990b) exhibits a 48% larger P_{O_2} drop across the CFR. This is explained by the fact that in the latter investigation $\dot{V}_{O_2}$ was 7% higher and effective capillary density was 27% smaller, together resulting in a 47% larger transcapillary O_2 flux.

A 27% difference in functional capillary density between data sets that have before been qualified as "similar" may be somewhat surprising. Yet, for the midcapillary profile from the muscle fiber model by Groebe and Thews (1990a, 1990b) there was no other choice: According to the data given in Table 2, a typical fiber in a maximally working muscle is surrounded by either three or four capillaries. As the model of Groebe and Thews (1990a, 1990b) assumes constant and maximal facilitation in all the muscle fiber cross section, correct results cannot be expected unless P_{O_2} in the fiber center does not exceed a few millimeters of mercury. This condition would not have been met if for the midcapillary profile four capillaries had been chosen. Therefore, the only alternatives were to omit the midcapillary profile or to use three capillaries, which gives the 27% difference in local functional capillary density. As was mentioned above, in Groebe and Thews (1990b) constant and maximal facilitation throughout the fiber was assumed. This is reflected in the fact that fiber P_{O_2} gradients near the capillary are much shallower than those from the other models. For the situation near the capillary origin—for which no calculations have been performed with the model of Groebe and Thews (1990b) because the assumption of constant and maximal facilitation is not satisfied there—there are considerable discrepancies between the resulting profiles. Whereas the dashed P_{O_2} distribution (Groebe, 1990) falls from 60 mm Hg in the RBC to 2 mm Hg in the fiber center, the one from the present model drops to 12 mm Hg only. Similarly, fiber P_{O_2} values near the venous capillary end calculated in Groebe (1990) are slightly higher than the ones from the present model. These are effects of staggering of capillary origins (which enhances/reduces transcapillary O_2 flux and hence P_{O_2} drops at capillary sites near the arterial/venous capillary ending) that were to be demonstrated in Groebe (1990). However, the assumed displacements of capillary origins by 700 μm in adjacent capillary layers are much larger than what would normally be expected (cf. Lund et al., 1987), and so are their effects on P_{O_2} distributions. Effects of this kind cannot be simulated in a capillary cylinder model and illustrate its limitations (see subsection 1).

In two recent papers geometrical assumptions in modeling O_2 transport to muscle tissue were evaluated. Piiper and Scheid (1986) studied Krogh- versus Hill-type models and concluded that "the real situation is intermediate but in the cases typical for skeletal muscle, i.e., capillary-to-fiber ratios not higher than 2 it is functionally closer to the Krogh than the solid cylinder model." Their observations have been reconfirmed and extended by Groebe and Thews (1990a): They used the already mentioned three-dimensional muscle fiber model that incorporates Mb-facilitated diffusion inside the fiber and a carrier-free region separating red blood cells and sarcolemma to demonstrate that

1. In order not to underestimate P_{O_2} drops near RBCs it is essential to consider the particulate nature of blood, i.e., to take account of plasma gaps separating adjacent RBCs.
2. A carrier-free region between RBC and fiber is important for understanding perierythrocytic P_{O_2} gradients.
3. A Hill-type model does not give an acceptable description of the P_{O_2} distributions for a capillary-to-fiber (c/f) ratio of 1 or of 2.
4. For a c/f ratio of 1, a Krogh-type model in which the O_2 fluxes within the carrier-free region are adapted according to Hellums (1977) yields almost identical P_{O_2} distributions as the three-dimensional model.
5. For a c/f ratio of 2, the profiles from a Krogh-type model show pronounced differences from those in the more comprehensive model.

In the present study, this last-named statement has been confirmed (P_{O_2} *profiles* for c/f ratios of 1 and 2 considerably deviate from one another; cf. Fig. 5) and is complemented by the observation that P_{O_2} *histograms* from both cases closely agree (Fig. 6).

In conclusion, the present paper develops and applies a model of O_2 supply to muscle that is of moderate mathematical complexity despite quite a respectable number of features included in it (which are listed in the Introduction). Thus, it can supply the physiologist who is not specialized

in the field of mathematical simulations with model equations for O_2 supply to muscle that may easily be programmed on a personal computer on the one hand, and still consider all those mechanisms that have been shown to be essential for a realistic description of red muscle O_2 supply on the other. By means of extensions made to the model it has been shown that under normal conditions the following simplifying assumptions do not corrupt the results:

1. O_2 flux is present only at locations adjacent to RBCs in the CFR and is uniform (with respect to the longitudinal coordinate) in the rest of the tissue.
2. Capillary domain cross sections are of circular shape.
3. There is no O_2 diffusion in parallel with the capillary direction.
4. The O_2 consumption rate is constant throughout the tissue and independent of P_{O_2} (or zero).

In order to assess the precision to which P_{O_2} distributions resulting from a mathematical model are correct, one needs to estimate the magnitude of errors propagated into the results from errors in the input data. The necessary information is supplied in a sensitivity analysis in which the derivatives of tissue P_{O_2} and of mean and standard deviation of the tissue P_{O_2} probability distribution with respect to the individual input parameters are calculated. Moreover, changes in mean tissue P_{O_2} brought about by plus or minus 50% changes in the input parameters are given. Discussion of the mechanisms underlying the pattern found for the various sensitivities reveals some fundamental principles governing O_2 supply to muscle tissue.

The present model's low requirements in computing time and its high transparency render it particularly suitable for tasks such as on-line estimates of P_{O_2} distributions for actual experimental situations, statistical evaluations (e.g., of large-scale heterogeneity effects) in which numerous model runs are required, and studies of the importance of individual parameter values and of general regularities and interrelations in the muscular O_2 supply system.

APPENDIX A: CALCULATING P_{O_2} DISTRIBUTIONS ON A COMPUTER

This appendix briefly outlines the steps to take in order to calculate P_{O_2} on a grid covering a longitudinal section through the capillary domain. This grid is defined by pairs (r_i, z_j) in which r_i, $i = 1, \ldots n$ are given radial coordinates (with $r_{i-1} < r_i$ and $r_n = R_K = 10^3(\pi fcd)^{-1/2}$ = Krogh radius) and z_j, $j = 0, \ldots m$ are equidistant longitudinal coordinates (with $z_0 = 0$, $z_m = L$ = capillary length, and grid spacing $\Delta z = L/m$). Moreover, let the index n_K be chosen such that r_{n_K} is an approximation to the Krogh radius at the actual longitudinal position. If capillary P_{O_2} is high enough to supply the entire capillary domain with oxygen, then, clearly, $n_K = n$; otherwise $n_K < n$. Starting at the arterial capillary end, one subsequently computes radial distributions $P_{O_2}(r_i)$, $i = 1, \ldots n_K$ for each longitudinal position z_j, $j = 0, \ldots m$ by iterating instructions 1–10 below.

Assume that the iteration has proceeded up to longitudinal position z_{j-1} and that for $z_j = j\Delta z$, $\mathscr{C} = \mathscr{C}(z_j)$ has been calculated. (For $j = 0$ let $\mathscr{C}(z_j) = \mathscr{C}_A$.) To find $P(r_i)$, $i = 1, \ldots n_K$ in the cross section at z_j take the following steps:

1. Determine $\mathscr{P}(\mathscr{C})$ by inverting Eq. 3 numerically or by applying one of the simplified formulas in Eq. 4. Calculate corresponding $\mathscr{S}(\mathscr{P}(\mathscr{C}))$ from the first of Eqs. 2.
2. Determine P_{RBC} from Eq. 17, using Φ_{RBC} from Eq. 16.
3. Determine $P(R_{CFR})$ from Eq. 19 and $P^*_{CFR} = \mathbf{P}^*(P(R_{CFR}))$ from Eq. 11.
4. Determine $P^*(r_{n_K})$ from Eq. 20.
5. If $P(R_{CFR}) < P_{crit}/2$ or $P^*(r_{n_K}) < \mathbf{P}^*(P_{crit}/2)$ decrement n_K by 1 and return to step 2.
6. Use Eq. 19 to calculate $P(r_i)$ at the selected radial coordinates, which are located in the CFR ($r_i \le R_{CFR}$).
7. Use Eqs. 20 and 21 to calculate $P(r_i)$ at the selected radial coordinates, which are located in the muscle cells ($r_i > R_{CFR}$) and for which $i \le n_K$.
8. If $j = m$, stop.
9. Calculate $\mathscr{C}(z_{j+1}) = \mathscr{C}(z_j + \Delta z) = \mathscr{C}(z) - (\dot{V}_{O_2}/\dot{Q}_{Cap})\pi(r^2_{n_K} - R^2_{CFR})\Delta z$ (cf. Eq. 15).
10. Increment j by 1 and return to step 1.

The iteration 2–5 for determining an approximation to the actual Krogh radius r_{n_K} from the one at the previous longitudinal position is not very precise because its scope is restricted to the predetermined grid values r_i, $i = 1, \ldots n$. Nevertheless it has been suggested here in place of more elaborate algorithms because it is simple to use and—if an n of ~100 or more is chosen—by far sufficiently precise for the present purposes.

APPENDIX B: SOLUTIONS FOR MORE COMPLEX CASES

In this appendix, the mathematics for assessing triangular capillary domains and axial diffusion are developed. To that end, a more general form of Eq. 12—the differential equation of steady state O_2 diffusion in the muscle cells—is to be solved for the effective O_2 partial pressure P^*. This solution is then specialized to satisfy the respective boundary and interface conditions.

It has been shown that O_2 diffusion in muscle is anisotropic in that diffusion along the muscle fiber axis is ~2.5 times faster than diffusion perpendicular to it (Homer et al., 1984). This anisotropy is accounted for in the following differential equation governing steady state O_2 diffusion in muscle:

$$\nabla(\mathbf{D}\nabla P^*) = \dot{V}_{O_2}/\alpha_M,$$

where $\mathbf{D}$ is a diagonal matrix specifying the diffusion coefficients along the x, y, and z axes. After transformation to cylindrical coordinates this differential equation becomes

$$\frac{D_{Mt}}{r}\frac{\partial}{\partial r}\left(r\frac{\partial P^*}{\partial r}\right) + \frac{D_{Mt}}{r^2}\frac{\partial^2 P^*}{\partial \varphi^2} + D_{Ml}\frac{\partial^2 P^*}{\partial z^2} = \frac{\dot{V}_{O_2}}{\alpha_M}, \qquad (23)$$

where D_{Mt} and D_{Ml} are the diffusion coefficients in the transverse and in the longitudinal directions, respectively. (D_{Mt} is equal to the D_M used above, and D_{Ml} is obtained as detailed in Groebe and Thews, 1990a.) All other quantities are as defined in Table 1. A particular solution of this inhomogeneous equation is given by

$$P^*_0(r) = \frac{\dot{V}_{O_2}}{2D_{Mt}\alpha_M}\left(\frac{r^2}{2} - R_K^2 \ln r\right) \qquad (24)$$

where $R_K = \sqrt{A/\pi}$ with the capillary domain cross sectional area A. By this equation, P^*_0 is uniquely determined up to a constant of integration, a_0.

The homogeneous equation is solved by separation of variables using the expression function $P^*(r, \varphi, z) = R(r)\Phi(\varphi)Z(z)$. For the separating variable λ^2, $\lambda \in \mathbb{R}$, we have

$$\frac{D_{Ml}}{D_{Mt}}\frac{d^2Z}{dz^2} = -\lambda^2 Z \Rightarrow Z(z) = \left\{\begin{matrix}\cos\\ \sin\end{matrix}\right\}\left(\lambda z\sqrt{\frac{D_{Mt}}{D_{Ml}}}\right)$$

$$\left(\left\{\begin{matrix}\cdots\\ \cdots\end{matrix}\right\} \text{ denote possible alternatives}\right)$$

and

$$\frac{r}{R}\frac{d}{dr}\left(r\frac{dR}{dr}\right) - \lambda^2 r^2 + \frac{1}{\Phi}\frac{d^2\Phi}{d\varphi^2} = 0.$$

Separating the latter equation again using the separating variable μ^2, $\mu \in \mathbb{R}$, we get

$$\frac{d^2\Phi}{d\varphi^2} = -\mu^2\Phi \Rightarrow \Phi(\varphi) = \begin{Bmatrix}\cos\\ \sin\end{Bmatrix}(\mu\varphi)$$

and

$$r\frac{d}{dr}\left(r\frac{dR}{dr}\right) - (\mu^2 + \lambda^2 r^2)R = 0 \Rightarrow R(r) = \begin{cases} r^{\pm\mu} & \lambda = 0 \\ \mathbf{Z}_\mu(i\lambda r) & \lambda > 0, \end{cases}$$

with the cylinder function $\mathbf{Z}_\mu$.

1. Triangular capillary domains

In the case of triangular capillary domains (cf. Fig. 4, bottom panel), Krogh's classical choice for the additive constant of integration a_0 in Eq. 24 yields the particular solution Eq. 20 of the inhomogeneous equation for which P^* at the CFR–fiber interface equals P^*_{CFR} ($P^*_{CFR} = \mathbf{P}^*(P(R_{CFR}))$ according to Eqs. 19 and 11 and for which O_2 flux into and O_2 consumption within the capillary domain are matched:

$$P^*_0 = P^*_{CFR} + \frac{\dot{V}_{O_2}}{2D_{Mt}\alpha_M}\left(\frac{1}{2}(r^2 - R^2_{CFR}) - R_K^2 \ln\frac{r}{R_{CFR}}\right). \quad (25)$$

As axial diffusion is neglected, there is no dependence of the solution of the homogeneous equation on the z coordinate, $Z(z)$ is constant and equal to 1, $\lambda = 0$, and the functions $R(r)$ are linear combinations of $r^{\pm\mu}$. In accordance with the above particular solution (Eq. 25), $R(r)$ is to vanish at $r = R_{CFR}$; hence $R(r) = (r/R_{CFR})^{-\mu} - (r/R_{CFR})^{\mu}$. Because of the assumed muscular geometry and of the requirement that all capillary domains be equal, the functions $\Phi(\varphi)$ need to be symmetric with respect to the bisectors of the angles of the triangular capillary domain. Consequently, the $\Phi(\varphi)$ are to be periodic (with a period of $(2/3)\pi$), μ has to be equal to an integral multiple of 3, and for a coordinate system in which the x axis is oriented as shown in Fig. 13, the harmonic functions need to be symmetric with respect to the x axis and thus are

$$P^*_n(r, \varphi) = \left(\left(\frac{r}{R_{CFR}}\right)^{-3n} - \left(\frac{r}{R_{CFR}}\right)^{3n}\right)\cos(3n\varphi), \quad n \in \mathbb{N}. \quad (26)$$

Using the functions P^*_0 and P^*_n from Eqs. 25 and 26, the solution for triangular capillary domains has the general form

$$P^*(r, \varphi) = P^*_0(r) + \sum_{n=1}^{\infty} a_n P^*_n(r, \varphi), \quad (27)$$

where a_n, $n \in \mathbb{N}$ are coefficients still to be determined.

Let s be the length of the edge $\overline{P_1P_2}$ of the triangular capillary domain cross section (cf. Fig. 13). Then s is related to R_K, the radius of the Krogh cylinder of same cross sectional area, as

$$s = 2\sqrt{\frac{\pi}{\sqrt{3}}}R_K,$$

and the coordinates of the corners P_1 and P_2 of the capillary domain cross section are given by

$$P_1 = \left(\frac{s}{2\sqrt{3}}, \frac{s}{2}\right), \qquad P_2 = \left(\frac{s}{2\sqrt{3}}, -\frac{s}{2}\right).$$

To satisfy the zero-flux boundary condition for triangular capillary domains, the coefficients a_n in Eq. 27 have to be determined such that the normal component of the gradient of P^* along the line $\overline{P_1P_2}$ (i.e., for $(r,\varphi) \in \overline{P_1P_2}$) vanishes:

$$\begin{aligned} 0 &\overset{!}{=} \left.\frac{\partial P^*}{\partial x}\right|_{(r,\varphi)\in\overline{P_1P_2}} \\ &= \frac{\partial P^*}{\partial r}\frac{\partial r}{\partial x} + \frac{\partial P^*}{\partial \varphi}\frac{\partial \varphi}{\partial x}\bigg|_{(r,\varphi)\in\overline{P_1P_2}} = \frac{\dot{V}_{O_2}}{2D_{Mt}\alpha_M}\left(r - \frac{R_K^2}{r}\right)\cos\varphi \\ &\quad - \sum_{n=1}^{\infty} a_n \frac{3n}{R_{CFR}}\left(\left(\frac{r}{R_{CFR}}\right)^{-3n-1} + \left(\frac{r}{R_{CFR}}\right)^{3n-1}\right)\cos(3n\varphi)\cos\varphi \\ &\quad + \sum_{n=1}^{\infty} a_n \frac{3n}{R_{CFR}}\left(\left(\frac{r}{R_{CFR}}\right)^{-3n-1} - \left(\frac{r}{R_{CFR}}\right)^{3n-1}\right)\sin(3n\varphi)\sin\varphi\bigg|_{(r,\varphi)\in\overline{P_1P_2}}. \end{aligned} \quad (28)$$

The condition $(r, \varphi) \in \overline{P_1P_2}$ is satisfied for

$$-\frac{\pi}{3} \le \varphi \le \frac{\pi}{3} \quad \text{and} \quad r = \frac{s}{2\sqrt{3}\cos\varphi}.$$

Substituting r accordingly and transforming Eq. 28 yields the following condition to be satisfied for all φ, $-\pi/3 \le \varphi \le \pi/3$):

$$\begin{aligned} \frac{\dot{V}_{O_2}R_{CFR}}{6D_{Mt}\alpha_M}\left(\frac{s}{2\sqrt{3}} - \frac{2\sqrt{3}}{s}R_K^2\cos^2\varphi\right) &= \sum_{n=1}^{\infty} a_n n\left(\left(\frac{2\sqrt{3}\cos\varphi R_{CFR}}{s}\right)^{3n+1}\cos((3n+1)\varphi)\right. \\ &\quad \left. + \left(\frac{s}{2\sqrt{3}\cos\varphi R_{CFR}}\right)^{3n-1}\cos((3n-1)\varphi)\right). \end{aligned}$$

This equation needs to be discretized with respect to φ, and the coefficients a_n must be determined numerically.

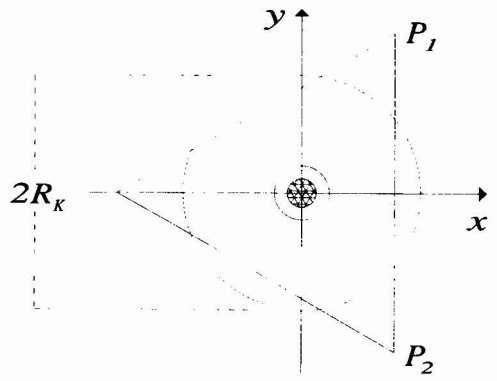

FIGURE 13 Positioning of triangular capillary domains relative to x and y coordinates: Solid circle, CFR containing RBC (cross-hatched); dashed circle of radius R_K, circular capillary domain of same cross-sectional area; P_1, P_2, corners of triangle.

2. Axial diffusion

In the case of axial diffusion in an axially symmetric capillary domain, there is no dependence of the solution upon the φ coordinate; hence $\Phi(\varphi)$ is constant and equal to 1 and $\mu = 0$. To satisfy the zero-flux boundary conditions at $z = 0$ and at $z = L$ (=capillary length), Z has to be equal to the cosine function and λ may take the values

$$\lambda = \frac{n\pi}{L}\sqrt{\frac{D_{Ml}}{D_{Mt}}}, \quad n \in \mathbb{N}.$$

On the other hand, the functions $R(r) = Z_0(i\lambda r)$ need to be chosen in a way to satisfy the zero-flux boundary condition at $r = R_K$. Consequently, the harmonic functions suitable for the solution to this boundary value problem are

$$P^*_n(r, z) = \cos\left(\frac{n\pi}{L}z\right)\left(\mathbf{I}_0\left(\frac{n\pi}{L}\sqrt{\frac{D_{Mt}}{D_{Ml}}}r\right) + b_n\mathbf{K}_0\left(\frac{n\pi}{L}\sqrt{\frac{D_{Mt}}{D_{Ml}}}r\right)\right), \quad n \in \mathbb{N}, \quad (29)$$

where $\mathbf{I}_0$ and $\mathbf{K}_0$ are the first- and second-kind modified Bessel functions of zero

order and

$$b_n = -\frac{\mathbf{I}_0'\left(\frac{n\pi}{L}\sqrt{\frac{D_{Mt}}{D_{Ml}}}R_K\right)}{\mathbf{K}_0'\left(\frac{n\pi}{L}\sqrt{\frac{D_{Mt}}{D_{Ml}}}R_K\right)}.$$

Using the notation P_0^* and P_n^* defined in Eqs. 24 and 29, we may write the general form of the solution:

$$P^*(r, z) = a_0 + P_0^*(r) + \sum_{n=1}^{\infty} a_n P_n^*(r, z), \tag{30}$$

where a_0 is an additive constant of integration. The coefficients a_n, $n \in \mathbb{N}_0$ need to be determined such that at the interface between carrier-free layer and muscle fiber P_{O_2} and O_2 flux are continuous.

Equation 9 relates the transcapillary O_2 flux per unit length (u.l.) of capillary, $\Phi_C(z) = -\dot{Q}_{Cap}(d\mathscr{C}(z)/dz)$ ($d\mathscr{C}/dz$ is the drop in mean capillary blood O_2 content per u.l. of capillary), to the O_2 consumed in a u.l. of capillary domain per unit of time, $\dot{V}_{O_2}(A - \pi R_{CFR}^2)$ (A is the capillary domain cross-sectional area). In the case of longitudinal diffusion, this relation is no longer correct in that longitudinal gradients give rise to diffusive O_2 flux in parallel with the direction of blood flow. Thus Φ_C will decrease from the arterial toward the venous capillary end, and the actual transcapillary O_2 flux, $-\dot{Q}_{Cap}(d\mathscr{C}(z)/dz)$, has to be substituted for any occurrence of $\dot{V}_{O_2}(A - \pi R_{CFR}^2)$ in the interface conditions. Other than in Eq. 10, the continuity of the O_2 flux at the interface between CFR and fiber therefore has to be expressed as

$$2\pi R_{CFR} D_{Mt} \alpha_M \left.\frac{\partial P^*(r, z)}{\partial r}\right|_{r=R_{CFR}} = \dot{Q}_{Cap}\frac{d\mathscr{C}(z)}{dz}. \tag{31}$$

Similarly, from Eq. 19 (which specifies the P_{O_2} in the CFR) one obtains the following equation for the continuity of the effective P_{O_2} at the interface:

$$P^*(R_{CFR}, z) = \mathbf{P}^*\left(P_{RBC}(z) + \frac{\dot{Q}_{Cap}}{2\pi D_{CFR}\alpha_{CFR} l_{RBC}} \ln\frac{R_{CFR}}{R_{RBC}}\frac{d\mathscr{C}(z)}{dz}\right), \tag{32}$$

where $P_{RBC}(z)$ is the P_{O_2} at the RBC surface at longitudinal position z (cf. Eqs. 15–17) and the function $\mathbf{P}^*(P)$ is as defined in Eq. 11. Substituting $P^*(r, \varphi)$ into Eq. 31 according to Eqs. 30, 24, and 29 yields

$$\frac{d\mathscr{C}(z)}{dz} = \frac{2\pi R_{CFR} D_{Mt}\alpha_M}{\dot{Q}_{Cap}}\left(\frac{\dot{V}_{O_2}}{2D_{Mt}\alpha_M}\left(R_{CFR} - \frac{R_K^2}{R_{CFR}}\right) + \sum_{n=1}^{\infty} a_n \cos\left(\frac{n\pi}{L}z\right)\frac{n\pi}{L}\sqrt{\frac{D_{Mt}}{D_{Ml}}}\left(\mathbf{I}_0'\left(\frac{n\pi}{L}\sqrt{\frac{D_{Mt}}{D_{Ml}}}R_{CFR}\right) + b_n\mathbf{K}_0'\left(\frac{n\pi}{L}\sqrt{\frac{D_{Mt}}{D_{Ml}}}R_{CFR}\right)\right)\right). \tag{33}$$

Substituting into Eq. 32 $P^*(r,\varphi)$ as above and $P_{RBC}(z)$ from Eqs. 17 and 16 (in which $\mathscr{S}$ has been replaced by $(\mathscr{C} - \alpha_{Blood}\mathscr{P}(\mathscr{C}))/HctC_{HS}$ according to Eq. 1 and $\dot{V}_{O_2}(A - \pi R_{CFR}^2)$ by the actual transcapillary O_2 flux $-\dot{Q}_{Cap}(d\mathscr{C}(z)/dz)$ results in

$$a_0 + \frac{\dot{V}_{O_2}}{2D_{Mt}\alpha_M}\left(\frac{R_{CFR}^2}{2} - R_K^2 \ln R_{CFR}\right) + \sum_{n=1}^{\infty} a_n \cos\left(\frac{n\pi}{L}z\right)\left(\mathbf{I}_0\left(\frac{n\pi}{L}\sqrt{\frac{D_{Mt}}{D_{Ml}}}R_{CFR}\right) + b_n\mathbf{K}_0\left(\frac{n\pi}{L}\sqrt{\frac{D_{Mt}}{D_{Ml}}}R_{CFR}\right)\right)$$
$$= \mathbf{P}^*\left(\mathscr{P}(\mathscr{C}(z))\left(1 + \frac{L_{RBC}\dot{Q}_{Cap}\sqrt{Hct}}{l_{RBC}\sigma_{RBC}\sqrt{D_{RBC}\alpha_{RBC}k\mathscr{P}(\mathscr{C}(z))n(\mathscr{C}(z) - \alpha_{Blood}\mathscr{P}(\mathscr{C}(z)))}}\frac{d\mathscr{C}(z)}{dz}\right) + \frac{\dot{Q}_{Cap}}{2\pi D_{CFR}\alpha_{CFR}l_{RBC}}\ln\frac{R_{CFR}}{R_{RBC}}\frac{d\mathscr{C}(z)}{dz}\right), \tag{34}$$

where $\mathscr{P}(\mathscr{C})$ is the equilibrium P_{O_2} pertinent to the capillary blood O_2 content $\mathscr{C}$ (as obtained by inversion of Eq. 3 or by Eq. 4 and

$$\mathscr{C}(z) = \mathscr{C}_A + \int_0^z \frac{d\mathscr{C}(\tilde{z})}{d\tilde{z}}\,d\tilde{z}, \tag{35}$$

with the blood O_2 content at the capillary origin, $\mathscr{C}_A$. These are the equations in the unknowns a_n, $n \in \mathbb{N}_0$, and $\mathscr{C}(z)$ to be solved for $z \in [0, L]$.

Equations 33–35 (together with Eqs. 3 or 4 and 11 for calculating $\mathscr{P}(\mathscr{C})$ and $\mathbf{P}^*(P)$, respectively) cannot be solved analytically but only numerically, for which purpose one has to discretize them with respect to the z coordinate (e.g., as $z_0, \ldots z_M$, $M \in \mathbb{N}$). A straightforward approach would be to substitute into Eq. 34 (which relates effective P_{O_2} at the inner and outer faces of the interface between CFR and muscle fiber) $d\mathscr{C}(z_i)/dz$ from Eq. 33 and $\mathscr{C}(z_i)$ from Eq. 35 and to use an algorithm for the solution of nonlinear equations (or of nonlinear least-squares problems) to find an optimal solution of this equation. This solution would be given by coefficients $a_0, \ldots a_N$ for a finite $N \in \mathbb{N}$, $N \le M$, which are determined such that the residuals of the substituted Eq. 34 at locations $z_0, \ldots z_M$ (or their sum of squares) are minimized. More specifically, on each function call by the minimization algorithm one would take the following steps: For a set of coefficients $a_0, \ldots a_N$ (which is provided by the algorithm) one would start at the capillary origin z_0 and proceed down the capillary to determine $d\mathscr{C}(z_i)/dz$ (from Eq. 33), $\mathscr{C}(z_i)$ (by numerical integration according to Eq. 35), and finally the values of $\mathscr{P}(\mathscr{C}(z_i))$ (from Eq. 3 or Eq. 4). Using $d\mathscr{C}(z_i)/dz$, $\mathscr{C}(z_i)$, and $\mathscr{P}(\mathscr{C}(z_i))$, one evaluates the residuals of Eq. 34 and returns them to the minimization algorithm. It is a severe drawback of this procedure that a rather large number N of unknowns $a_0, \ldots a_N$ in the nonlinear problem is required (~30–50) to achieve an acceptable approximation. As a consequence, a global best approximation is hardly ever found, and the algorithm mostly converges to a local minimum only—with the effect that for the final approximation returned by the least-squares algorithm, residuals are still large (a few percent), and the outer P_{O_2} at the interface between CFR and muscle cell considerably oscillates about the values of the inner P_{O_2} (which smoothly drop along the capillary).

Nevertheless, this procedure gives a general idea of what courses of the transcapillary O_2 flux along the capillary, $\Phi_C(z) = -\dot{Q}_{Cap}(d\mathscr{C}(z)/dz)$, to expect. This information can be used to guess expression functions $\Phi_{Cj}(z)$, $j = 1, \ldots K$ that are suitable for approximating these courses of $\Phi_C(z)$ and to express transcapillary O_2 flux as a linear combination thereof: $\Phi_C(z) = \sum_j \mathscr{C}_j\Phi_{Cj}(z)$. As above, the coefficients c_j for an optimal solution of the problem may be found by a nonlinear least-squares algorithm; however, this time the residuals of Eq. 33 are minimized instead of the ones of Eq. 34: Using a current course of $\Phi_C(z)$ (which is determined by a set of coefficients c_j provided by the algorithm) one computes the drops in O_2 concentration $d\mathscr{C}(z_i)/dz = -\dot{Q}_{Cap}^{-1}\sum_j c_j\Phi_{Cj}(z_i)$ at positions $z_0, \ldots z_M$ and $\mathscr{C}(z_i)$ (from Eq. 35) and the effective P_{O_2} along the inside of the CFR–tissue interface (right-hand side of Eq. 34 and Eq. 11). The left-hand side of Eq. 34 depends on the unknown coefficients $a_0, \ldots a_N$, but in a linear fashion only. Therefore, even for large values of N, the coefficients $a_0, \ldots a_N$ may easily be determined by a Fourier analysis (for suitable $N = M$ even by a fast Fourier transform) such that residuals of Eq. 34 are minimized. With the resulting optimal set of coefficients $a_0, \ldots a_N$, the residuals in the equations for $d\mathscr{C}(z_i)/dz$ (Eq. 33) at longitudinal coordinates $z_0, \ldots z_M$ may be calculated and returned to the nonlinear least-squares algorithm. This procedure has the advantage that for $K = 9$ coefficients c_j and for the same discretization $z_0, \ldots z_M$ as above, the optimum residual is, on an average, only approximately 0.1–0.2%.

Acknowledgment

With this paper, the author wishes to thank his teacher Prof. Dr. Dr. G. Thews for his support and his assistance on countless occasions over many years. Moreover, it is a pleasure and a sorrowful obligation for the author

to express his gratitude toward the late Prof. Dr. C. Honig for his many stimulating suggestions and his unremitting constructive criticism. Carl, I will always keep you in loving memory.

REFERENCES

Altman, P. L., and D. S. Dittmer. 1972. Biology Data Book. Federation of American Societies for Experimental Biology, Bethesda.

Baylor, S. M., and P. C. Pape. 1988. Measurement of myoglobin diffusivity in the myoplasm of frog skeletal muscle fibres. *J. Physiol. (London)* 406:247–275.

Clark, A., and P. A. A. Clark. 1986. The end-points of the oxygen path: transport resistance in red cells and mitochondria. *Adv. Exp. Med. Biol.* 200:43–47.

Clark, A., W. J. Federspiel, P. A. A. Clark, and G. R. Cokelet. 1985. Oxygen delivery from red cells. *Biophys. J.* 47:171–181.

Connett, R. J., and C. R. Honig. 1989. Regulation of $\dot{V}_{O_2}$ in red muscle: do current biochemical hypotheses fit in vivo data? *Am. J. Physiol.* 256: R898–R906.

Connett, R. J., C. R. Honig, T. E. J. Gayeski, and G. A. Brooks. 1990. Defining hypoxia: a systems view of $\dot{V}_{O_2}$, glycolysis, energetics, and intracellular P_{O_2}. *J. Appl. Physiol.* 68:833–842.

Eriksson, E., and M. Myrhage. 1972. Microvascular dimensions and blood flow in skeletal muscle. *Acta Physiol. Scand.* 86:211–222.

Federspiel, W. J. 1986. A model study of intracellular oxygen gradients in a myoglobin-containing skeletal muscle fiber. *Biophys. J.* 49:857–868.

Federspiel, W. J., and A. S. Popel. 1986. A theoretical analysis of the effect of the particulate nature of blood on oxygen release in capillaries. *Microvasc. Res.* 32:164–189.

Gayeski, T. E. J., R. J. Connett, and C. R. Honig. 1987. Minimum intracellular P_{O_2} for maximum cytochrome turnover in red muscle in situ. *Am. J. Physiol.* 252:H906–H915.

Gayeski, T. E. J., and C. R. Honig. 1986. O_2 gradients from sarcolemma to cell interior in red muscle at maximal $\dot{V}_{O_2}$. *Am. J. Physiol.* 251: H789–H799.

Gayeski, T. E. J., and C. R. Honig. 1988. Intracellular P_{O_2} in long axis of individual fibers in working dog gracilis muscle. *Am. J. Physiol.* 254:H1179–H1186.

Groebe, K. 1990. A versatile model of steady state O_2 supply to tissue. Application to skeletal muscle. *Biophys. J.* 57:485–498.

Groebe, K., and G. Thews. 1986. Theoretical analysis of oxygen supply to contracted skeletal muscle. *Adv. Exp. Med. Biol.* 200:495–514.

Groebe, K. 1992. Factors important in modelling oxygen supply to red muscle. In Oxygen Transport in Biological Systems. S. Egginton and H. F. Ross, editors, Vol. 51 of SEB Seminar Series 51. Cambridge University Press, Cambridge. 231–252.

Groebe, K., and G. Thews. 1989. Effects of red cell spacing and red cell movement upon oxygen release under conditions of maximally working skeletal muscle. *Adv. Exp. Med. Biol.* 248:175–185.

Groebe, K., and G. Thews. 1990a. Role of geometry and anisotropic diffusion for modelling P_{O_2} profiles in working red muscle. *Respir. Physiol.* 79:255–278.

Groebe, K., and G. Thews. 1990b. Calculated intra- and extracellular P_{O_2} gradients in heavily working red muscle. *Am. J. Physiol.* 259: H84–H92.

Hellums, J. D. 1977. The resistance to oxygen transport in the capillaries relative to that in the surrounding tissue. *Microvasc. Res.* 13:131–136.

Homer, L. D., J. B. Shelton, C. H. Dorsey, and T. J. Williams. 1984. Anisotropic diffusion of oxygen in slices of rat muscle. *Am. J. Physiol.* 246: R107–R113.

Honig, C. R., T. E. J. Gayeski, W. Federspiel, A. Clark, and P. Clark. 1984. Muscle O_2 gradients from hemoglobin to cytochrome: new concepts, new complexities. *Adv. Exp. Med. Biol.* 169:23–38.

Honig, C. R., and C. L. Odoroff. 1981. Calculated dispersion of capillary transit times: significance for oxygen exchange. *Am. J. Physiol.* 240: H196–H208.

Hoofd, L., Z. Turek, and J. Olders. 1989. Calculation of oxygen pressures and fluxes in a flat plane perpendicular to any capillary distribution. *Adv. Exp. Med. Biol.* 248:187–196.

Jürgens, K. D., T. Peters, and G. Gros. 1994. Diffusivity of myoglobin in intact skeletal muscle cells. *Proc. Natl. Acad. Sci. USA.* 91:3829–3833.

Klitzman, B., and B. R. Duling. 1979. Microvascular hematocrit and red cell flow in resting and contracted striated muscle. *Am. J. Physiol.* 237:H481–H490.

Laughlin M. H. 1991. Heterogeneity of blood flow in striated muscle. In The Lung, Scientific Foundations. R. G. Crystal, J. B. West, and others, editors. Raven, New York. 1507–1516.

Lund, N., D. H. Damon, D. N. Damon, and B. R. Duling. 1987. Capillary grouping in hamster tibialis anterior muscles: Flow patterns, and physiological significance. *Int. J. Microcirc Clin. Exp.* 5:359–372.

Martin, E. G., E. C. Wooley, and M. Miller. 1932. Capillary counts in resting and active muscles. *Am. J. Physiol.* 100:407–416.

Mendez, J., and A. Keys. 1960. Density and composition of mammalian muscle. *Metabolism* 9:184–188.

Piiper, J., and P. Scheid. 1986. Cross-sectional P_{O_2} distributions in Krogh cylinder and solid cylinder models. *Respir. Physiol.* 64:241–251.

Zander, R. 1975. Cellular oxygen concentration. *Adv. Exp. Med. Biol.* 75: 463–467.

Zweifach, B. J., and H. H. Lipowsky. 1984. Pressure-flow relations in blood and lymph microcirculation. In Handbook of Physiology, Sect. 2: The Cardiovascular System, Vol. IV: Microcirculation. E. M. Renkin and C. C. Michel, editors. American Physiological Society, Bethesda. 251–307.